We are IntechOpen,
the world's leading publisher of
Open Access books
Built by scientists, for scientists

6,900
Open access books available

186,000
International authors and editors

200M
Downloads

Our authors are among the

154
Countries delivered to

TOP 1%
most cited scientists

12.2%
Contributors from top 500 universities

CLARIVATE ANALYTICS
BOOK CITATION INDEX
INDEXED

WEB OF SCIENCE™

Selection of our books indexed in the Book Citation Index
in Web of Science™ Core Collection (BKCI)

Interested in publishing with us?
Contact book.department@intechopen.com

Numbers displayed above are based on latest data collected.
For more information visit www.intechopen.com

CVD-Made Spinels: Synthesis, Characterization and Applications for Clean Energy

Patrick Mountapmbeme Kouotou, Guan-Fu Pan and
Zhen-Yu Tian

Additional information is available at the end of the chapter

Abstract

To reduce emissions and protect environment from pollution caused by volatile organic compounds (VOCs) and CO, catalytic oxidation can be applied as an efficient and promising technique. This review provides a novel and facile strategy to synthesize spinel-type and non-spinel-type transition metal oxides (TMOs). Specifically, single (Co_3O_4, α-Fe_2O_3, Mn_3O_4, CuO, Cu_2O and Cr_2O_3) and binary ($Co_{3-x}Cu_xO_4$, $Co_{3-x}Mn_xO_4$ and $Co_{3-x}Fe_xO_4$) TMOs have been prepared using pulsed spray evaporation chemical vapor deposition approach (PSE-CVD). PSE-CVD offers several advantages over conventional methods, such as relatively low cost, simplicity and high throughput, which makes it a promising strategy. Moreover, the PSE delivery system allows using less stable precursors and permits improving the reproducibility of the film properties with tailored compositions. The above listed TMOs prepared by PSE-CVD were successfully tested as catalysts toward the complete oxidation of some real fuels such as CO, C_2H_2, C_3H_6, n-C_4H_8 and C_2H_6O as representatives of VOCs and industrial exhaust streams. The active TMOs explored in this review could be potential catalysts candidates in one of the research areas that are currently under scrutiny, as the battle for the future of energy and environment involves the generation and application of clean energy.

Keywords: clean energy, VOCs, biofuels, catalytic oxidation, PSE-CVD, TMOs, in-situ diagnostic; mechanism

1. Introduction

Volatile organic compounds (VOCs) are widely recognized as the major contributors to the global air pollution [1]. VOCs are composed of a variety of substances, which may be either natural or of anthropogenic origin from different human activities such as transportation and many factories or industrial processes including chemical, power and pharmaceutical plants, gas stations, petroleum refining, printing, food processing, automobile, as well as textile manufacturing [2]. The volatility of the emission from the above-listed sources enables them to diffuse more or less away from their place of issue, thus causing direct and indirect impacts on human health, animals and nature. In recent years, with the rapid increase of population, industrialization, transportation and urbanization, extremely severe and persistent haze pollution has been frequently observed in developing countries. For example, by 2020, VOCs emissions are predicted to increase by 49% relative to 2005 levels in China [3]. Therefore, in addition to the increasingly stringent controls for VOCs emissions level, it is urgent to develop and apply approaches to accelerate the reduction in VOCs emissions which is also vital in the context of climate change.

VOCs include a wide range of compounds such as aromatic and aliphatic hydrocarbons, alcohols, ketones, aldehydes, which are not easy to be oxidized. Abatement by catalytic oxidation appears to be a preferable technique compared to the thermal incineration in reducing VOCs. In fact, thermal oxidation is known to be expensive since it requires a substantial energy input to destroy dilute gas phase containing VOCs at relatively high temperature (750°C) which favors the formation of toxic by-products. In contrast, catalytic oxidation allows operating at much lower temperatures (200–500°C) and leads to none or negligible NO_x formation in the combustion chamber. More importantly, catalytic oxidation can destroy VOCs and convert them into harmless CO_2 and H_2O [4]. In addition, the selectivity of catalytic oxidation could be well controlled. However, to achieve deep oxidation at mild temperature, highly active, nonselective and stable catalysts for extended periods of time are required.

Nowadays, the selection of catalyst for various organic pollutants abatement has been the subject of many studies, although the optimization of catalyst formulation does not appear to be an easy task. Noble metals and transition metal oxides (TMOs) have been widely explored in most commercial applications [5–11]. Noble metals are very active at low temperature, but their use is limited due to the high price, low thermal stability and tendency to poisoning [12]. In contrary, TMOs are considered as suitable alternatives because of higher thermal stability and lower price [13]. Among TMOs, single and mixed oxides, such as manganese and cobalt oxides, perovskites, zirconia-based catalysts, have been claimed for their effectiveness in VOCs oxidation [14–19]. In particular, Co_3O_4-based catalysts, which have been studied several decades ago regarding the high activity for CO and VOCs oxidation [20–22], have received again considerable attention in the recent years [23–28]. However, the physico-chemical and catalytic properties of TMOs thin films can be modulated with respect to the morphology, surface and bulk composition as well as metallic ratio, which are strongly dependent upon the

preparation approaches and experimental conditions [29–32]. Thus, suitable synthesis route for the deposition of thin films of high purity and crystallinity is urgently needed.

In recent years, great efforts have been made to the development of efficient TMOs synthesis methods, including sol-gel [33], thermal decomposition [34], hydrothermal synthesis, electro-deposition [35] and pulsed spray evaporation chemical vapor deposition (PSE-CVD) [23–28]. Among these techniques, PSE-CVD shows the benefit of being a reliable one-pot method for the growth of complex oxides with controlled composition, since most of the functional oxides contain more than two elements in their structures and further tuning of their properties requires controlled doping ratio. The strategy of using multiple precursors in a single liquid feedstock and its combination with PSE-CVD have been proved to be a rationally controllable route for the growth of functionally mixed oxides such as spinels and perovskites [36]. In addition to complex oxides structures, PSE-CVD synthesis route offers also the potential to produce nano-scale layers of pure metals, metal carbides as well as alloys, which presents a large variety of potential applications.

In this review, we mainly focus on the progress made in the deposition of single and binary metal oxides-containing thin films using gas-phase processes namely PSE-CVD for complete catalytic oxidation of CO and VOCs operating at low temperature generally below 500°C or even at much lower temperature. Following a general introduction, a brief recall of the mechanisms involved in the catalytic oxidation over TMOs is described. The main sections deal with catalytic oxidation of VOCs over single and mixed TMOs followed by remarks and perspectives. We examined several typical metal oxides that are widely studied as the essential components for catalytic oxidation of CO and VOCs and explored the effect of some important influencing factors such as the redox properties, composition, doping, film morphology and the particle size of the metals oxides. The specific mechanisms involved in the catalytic activity process toward low-temperature VOC oxidation are discussed.

2. Reaction mechanisms with TMOs

Oxides-type catalysts made of transition metals are well known to selectively catalyze a large number of chemical processes. Most often, these oxides are used in the form of powder or supported thin film for oxidation reactions in the chemical industry or in automotive emission control. Although low-temperature catalytic oxidation of CO was intensively studied and the mechanism has been well addressed, it is still difficult to extend the results obtained from this reaction to catalytic oxidation of VOCs due to the different properties of pollutants and reaction conditions [37]. Depending on the partial reaction order, different reaction mechanisms have been proposed for CO and VOCs oxidation. First, the Langmuir mechanism states that the reaction occurs via the so-called Eley-Rideal (ER) process in which the reaction proceeds via a collision between an impinging gas-phase molecule and an adsorbed species, the controlling step being the reaction between an adsorbed molecule and a molecule from the gas phase [38]. The ER process for simple molecule such as CO can be schematically represented in **Scheme 1**.
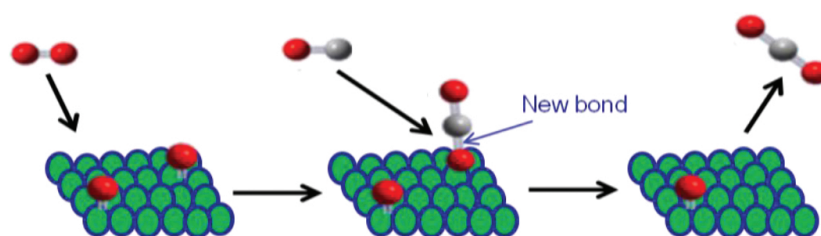
Scheme 1. Schematic illustration of the ER process for CO oxidation.

Second, the Langmuir-Hinshelwood (LH) mechanism indicates the reaction happens through interactions among the adsorbed molecules, radicals or fragments of the reactant molecules [39] (see **Scheme 2**). According to LH, the controlling step is the surface reaction between two adsorbed molecules on analogous active sites.
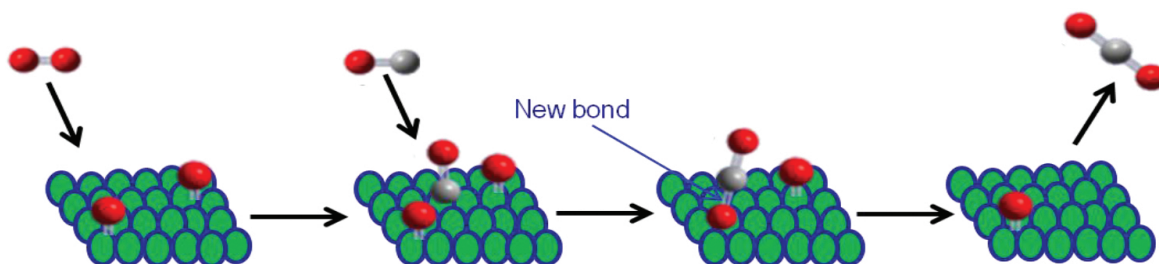
Scheme 2. Schematic illustration of the LH process for CO oxidation.

Finally, the Mars-van Krevelen (MvK) mechanism [40] points out the lattice oxygen enters the reaction sequences, caused an oxidation-reduction sequence in the reaction of the reactant molecules and oxygen on different redox sites as schematically represented in **Scheme 3**. This mechanism has been widely accepted and used for the oxidation of a series of organic compounds.
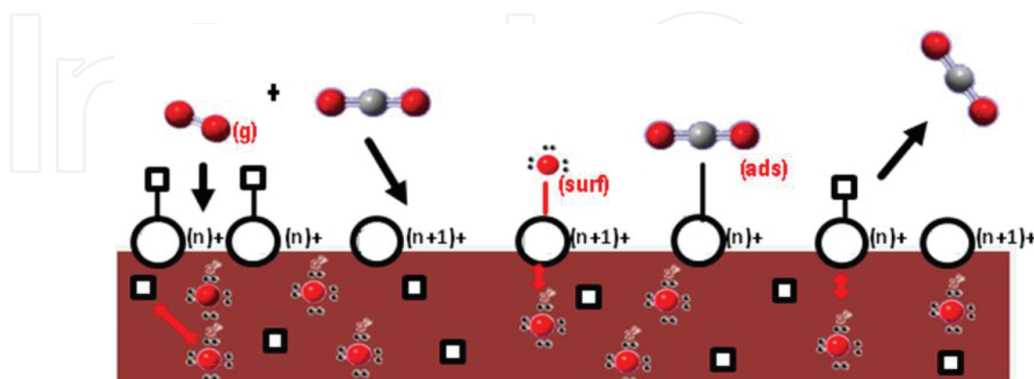
Scheme 3. Illustration of the MvK mechanism for CO oxidation.

For the transition metal catalysts either in single oxide (Co_3O_4, CuO/Cu_2O, Fe_2O_3, Cr_2O_3 as well as Mn_3O_4) or in binary oxide phase (Co-Cu, Co-Fe, Co-Mn and so on), it has been widely

demonstrated and recognized that the determinant factors affecting their activities and performances toward complete oxidation of CO and VOCs are the formation of highly active oxygen species activated by the oxygen vacancies in addition to the close relationship between redox properties, oxygen vacancies and the bulk oxygen mobility through the Mars-van Krevelen (MvK) mechanism. In general, the MvK mechanism can proceed in two successive steps in terms of the cyclic reaction, namely the transfer of the bulk oxygen ions to the surface sites being the first step for the decomposition of bulk oxides and then the recovering of the bulk oxide. In this first step, oxygen vacancies on the catalyst surface are reduced as they react with the organic molecules. Therefore, the presence of surface oxygen vacancies plays a crucial role in the decomposition of bulk oxide. In the second step, the preformed reduced site is immediately regenerated through the consumption of gaseous oxygen or the transfer of oxygen atoms from the bulk to the surface, that is, the oxygen molecules compete with the bulk lattice oxygen for the surface oxygen vacancies, resulting in the inhibition of the bulk oxide decomposition process [41]. Since the catalyst is reduced in the first step and then reoxidized in the second step, this mechanism is also known as the redox mechanism.

3. Tailored synthesis, characterization and application of single and binary oxides

The most active oxides frequently used are made of Ag, V, Cr, Mn, Fe, Co, Ni and Cu [42]. In fact, these *n*-type and *p*-type metal oxides are generally active catalysts (particularly *p*-type) for deep oxidation since they are electron-deficient in the lattice and conduct electrons by means of positive "holes" [37]. In addition, the adsorbed oxygen species generally observed at their surfaces might participate in the reaction sequences together with the lattice oxide ions to improve the catalysts' performances. Therefore, numerous investigations on the development of TMOs catalysts are mainly focused on this type of oxides. Several *n*-type and *p*-type single oxides such as Co_3O_4 [23], α-Fe_2O_3, Mn_3O_4 [43], CuO [44], Cu_2O [45] and Cr_2O_3 [46] have been prepared via PSE-CVD and successfully tested as active catalysts toward total oxidation of some real fuels such as CO, C_2H_2, C_3H_6, *n*-C_4H_8 and C_2H_6O as representatives of industrial exhaust stream or VOCs. Among these oxides mentioned above, a few of them seem to be particularly promising.

3.1. CO and VOCs oxidation over PSE-CVD made single oxide catalysts

3.1.1. Cobalt oxide with spinel structure

Cobalt oxide has a spinel structure and its formula can be written as CoO-Co_2O_3, or Co_3O_4. It presents an ideal spinel structure in which Co^{2+} cations occupy one-eighth of the tetrahedral sites, Co^{3+} cations occupy half of the octahedral sites and 32 sites are occupied by O^{2-} ions [47]. Spinel Co_3O_4 has been used broadly and successfully for the destruction of CO and hydrocarbons compounds [48] and is claimed to be one of the most active catalysts in destruction of these compounds. The performances of some Co-based catalysts seem to be comparable to

some noble metal catalysts. The high activity of Co_3O_4 is likely to be related to the relatively low enthalpy of vaporization (ΔH_{vap}) of O_2 [47]. Therefore, the Co–O bond strength of Co_3O_4 can affect desorption of lattice oxygen [49]. For example, CO frequently seems to react with pre-adsorbed or lattice oxygen to give CO_2, which may further react to form surface carbonate species.

Kouotou et al. have studied the total oxidation of C_3H_6 and CO over PSE-CVD made spinel Co_3O_4 deposited on stainless steel grid mesh [23] and the as-deposited Co_3O_4 catalysts exhibited good activity compared with the reaction over non-coated mesh (NCM) as blank experiment (see **Figure 1**). The total conversion of the investigated compounds to CO_2 was obtained respectively at around 380°C for C_3H_6 and 350°C for CO, which gives an obvious temperature shift relative to the NCM. This result shows that Co_3O_4 prepared by PSE-CVD was active for total oxidation of CO and C_3H_6. The catalytic performance of Co_3O_4 toward the oxidation of CO and C_3H_6 was attributed to the abundance of active Co^{3+}/Co^{2+} cations and oxygen vacancies generally present at the surface of such materials. Co^{3+}/Co^{2+} cations and oxygen vacancies were suggested to act as active sites for the oxidation process and are key parameters governing catalytic process during the total conversion rate of CO and C_3H_6.
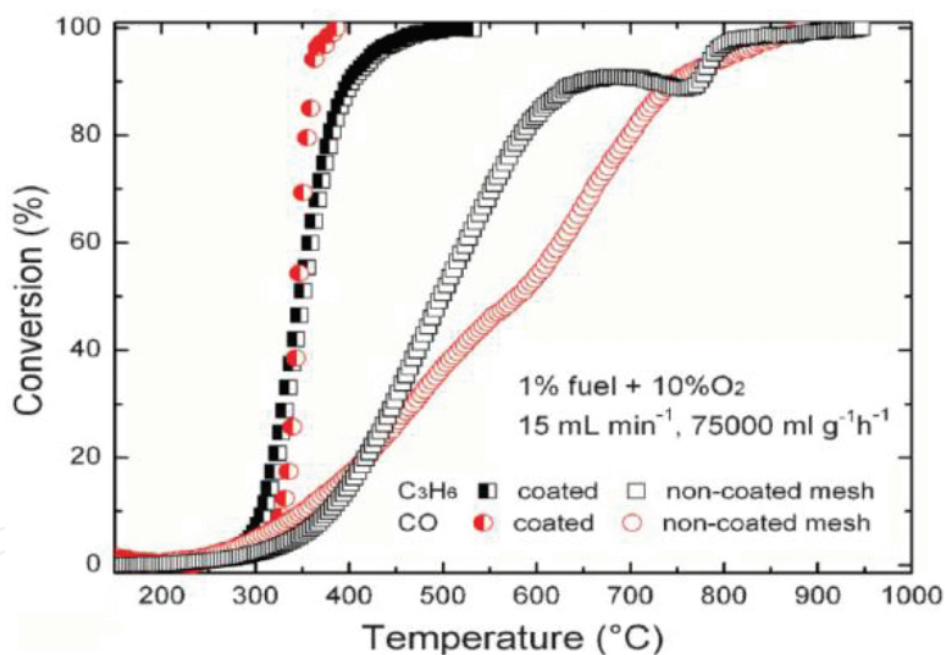

Figure 1. Light-off curves of C_3H_6 and CO catalytic conversion over grid-mesh of stainless steel coated with Co_3O_4 and non-coated mesh as reference. Reproduced from [23] with permission. Copyright 2013, the Royal Society of Chemistry.

3.1.2. Hematite

Hematite, known as iron oxide (α-Fe_2O_3), has been extensively studied because of its excellent chemical stability, natural abundance, low cost, relatively nontoxic and environmentally benign [50]. As an important precursor, α-Fe_2O_3 is the most stable iron oxide phase, featuring some unique properties such as n-type semiconductor and magnetic as well as corrosion-

resistant properties [51]. α-Fe$_2$O$_3$ can be converted into other functional materials such as maghemite (γ-Fe$_2$O$_3$) and magnetite (Fe$_3$O$_4$) [52]. These properties have driven α-Fe$_2$O$_3$ in numerous promising applications. Among them, application of α-Fe$_2$O$_3$ as catalysts caught wide attention. A systematic study was carried out by Walker et al. [53] who evaluated the possible application of iron catalysts for automotive emission control. Despite the promising results, α-Fe$_2$O$_3$ has been scarcely tested as catalyst for the abatement of CO and VOCs. Recently, α-Fe$_2$O$_3$ thin films have been selectively prepared by PSE-CVD approach and successfully tested against the low-temperature catalytic oxidation of CO and propene. As a reference, the reaction was first performed on NCM in the temperature range of 180–950°C. An identical mesh coated with 20 mg α-Fe$_2$O$_3$ was then tested under the same inlet gas conditions, but raising the temperature only to 500°C, which is the lattice stability temperature limit of α-Fe$_2$O$_3$ [54]. In the presence of α-Fe$_2$O$_3$, the conversion of CO started at ~220°C and complete conversion occurred at 398°C, while these values were shifted to ~300 and 930°C on NCM, respectively (see **Figure 2**). It should be mentioned that the reusability of the obtained α-Fe$_2$O$_3$ films and reproducibility of their catalytic performance were satisfactory within experimental uncertainty. The obtained results were compared to results reported by Walker et al. [53] who used unsupported Fe$_2$O$_3$ and several supported catalysts for CO oxidation. The temperature at 50% of CO conversion (defined as T_{50}) was found to be 398°C with Fe$_2$O$_3$ [53], while PSE-CVD made α-Fe$_2$O$_3$ thin films [55] enabled 50% conversion of CO to CO$_2$ at 320°C, 78°C lower than Fe$_2$O$_3$ from Walker et al.'s work, revealing the better catalytic performance of the PSE-CVD deposited thin films. More details regarding the comparison can be found in **Table 2** (see Section 2.1.6).
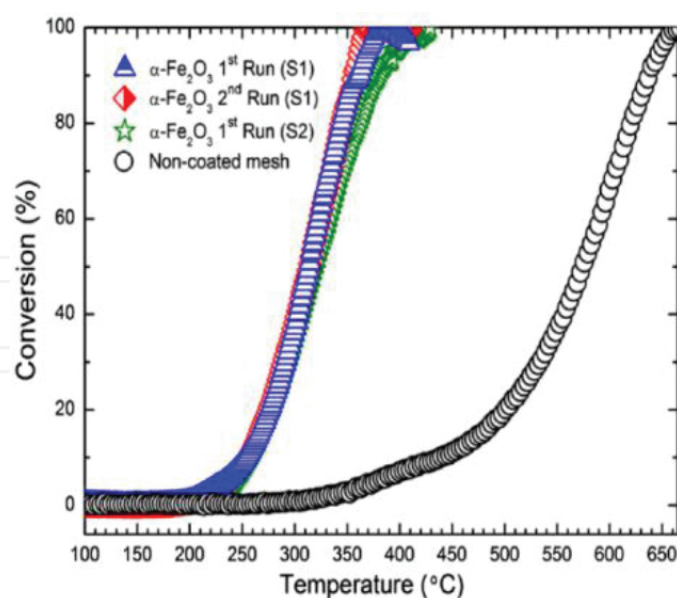

Figure 2. CO conversion profiles over stainless steel grid meshes coated with α-Fe$_2$O$_3$ films at a WHSV of 45,000 g$_{cat}^{-1}$ h^{-1}. Two samples (S1 and S2) prepared at the same conditions were tested. First run and 2nd run are the catalytic tests performed for the first and second time, respectively. The performance for NCM is included as a reference. Reproduced from [55] with permission. Copyright 2013, Elsevier.

The reaction mechanism involved in CO oxidation over various Fe_2O_3 surfaces has been widely discussed in the literature [56–58]. As an example, a suprafacial mechanism describing the oxidation of CO over hematite has been proposed by Kandalam et al. [57] and was suggested to be applicable to the catalytic reaction with PSE-CVD made hematite [55]. According to Kandalam et al. [57], CO molecule first adsorbs onto hematite, weakening a Fe-O bond near the crystal surface and then, a second CO molecule adsorbs and forms CO_2 by breaking the weakened Fe–O bond [57]. As hematite films are composed of a bulk and surface region on which active adsorption sites exist, part of these sites could be occupied by trapped oxygen atoms, which can originate either via dissociation of adsorbed oxygen during the oxidation reaction or via diffusion from the lattice to the surface. In addition, the number of surface iron atoms with which the adsorbed O_2 can interact was earlier reported to play a significant role [59].

Besides CO oxidation, deep oxidations of C_3H_6 have been achieved at low temperature over a series of α-Fe_2O_3 thin films coated at different temperature on stainless steel. The effect of the deposition temperature on the film morphology and redox properties has been systematically investigated and their influences on the catalytic oxidation of C_3H_6 have been clearly demonstrated [54]. Since the samples presented different redox behavior that is the temperature-programmed reduction (TPR), oxygen states distribution (lattice and adsorbed) obtained by the X-ray photoelectron spectroscopy (XPS) and morphology by helium ion microscopy (HIM, see **Figure 3**) [54], the catalytic tests were performed for all samples. The objective was to investigate these effects on the catalytic properties. To analyze the catalytic behavior after reoxidation as a prerequisite for application in consecutive cycles, the catalytic conversion of C_3H_6 was carried out both before and after pretreatment of the catalyst under oxygen flow. This was done because of the large amount of adventitious carbon, C–O and O–C=O type moieties detected at the surface of the samples prepared at 400 and 450°C (see **Table 1** and **Figure 3**) would be expected to limit their performance by forming a barrier layer between the active sites of the catalysts and the reactant molecules. The catalytic tests on fresh samples were performed over catalysts prepared at 350 and 450°C which present the lowest and the highest concentration of carbonaceous species, respectively. In addition, all pretreated samples were used at least twice in the catalytic tests to assess the reproducibility, as shown in **Figure 4**. **Figure 4** displays the light-off curves of C_3H_6 conversion obtained with α-Fe_2O_3 fresh samples (**Figure 4a**) and with α-Fe_2O_3 pretreated samples (**Figure 4b**). With fresh samples, catalyst (CAT) prepared at 350°C (CAT$_{350}$) with lower adsorbed species presents better performance than CAT$_{450°C}$. For each sample, the conversion begins at around 250°C. Temperatures for 10, 50 and 90% C_3H_6 conversion were presented for fresh and pretreated samples. The film prepared at 350°C was the most active one regarding the conversion profile as a function of temperature, followed by the films obtained at 400 and 450°C, respectively (**Table 1**). The experiments were repeated and the results were reproducible (**Figure 4b**). α-Fe_2O_3 thin films present competitive activity to that reported for supported noble metals. As an example, with only 20 mg of α-Fe_2O_3 deposited at 350°C, the oxidation of 50% of propene was reached at 331°C, whereas that of 200 mg Au/Al_2O_3 and $La_{1.7}Sr_{0.3}CuO_4S_{0.2}$ was obtained at 365 and 419°C, respectively. More details regarding the comparison can be found in **Table 2** (see Section 2.1.6).
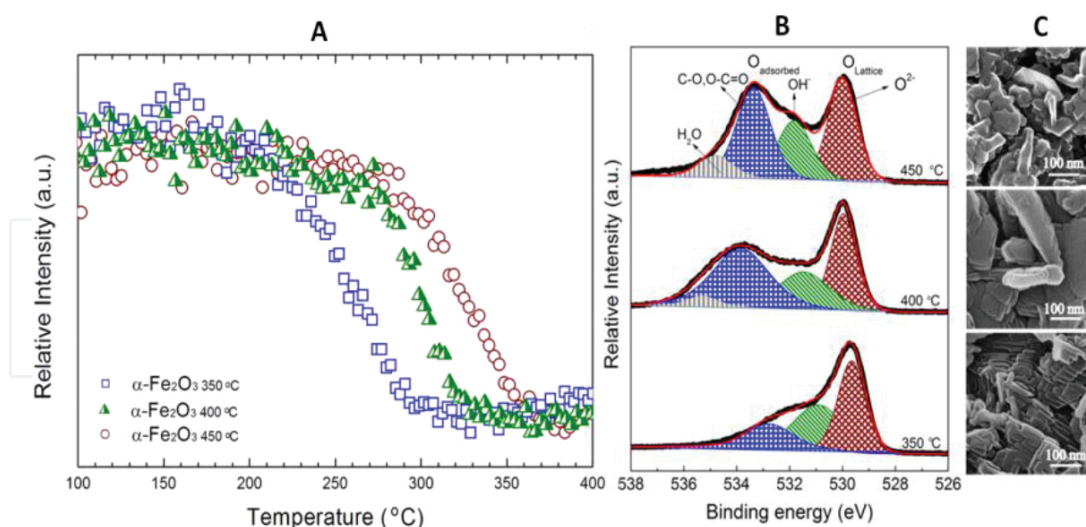
Figure 3. TPR profiles obtained for α-Fe$_2$O$_3$ thin films, showing variation of the reduction properties in function of deposition temperature (A); XPS O 1s core-shell for α-Fe$_2$O$_3$ thin films, thin and thick lines are fitted and experimental results respectively (B) and HIM images of α-Fe$_2$O$_3$ thin films coated on stainless steel at different temperatures (C). Reproduced from [54] with permission. Copyright 2013, the Royal Society of Chemistry.
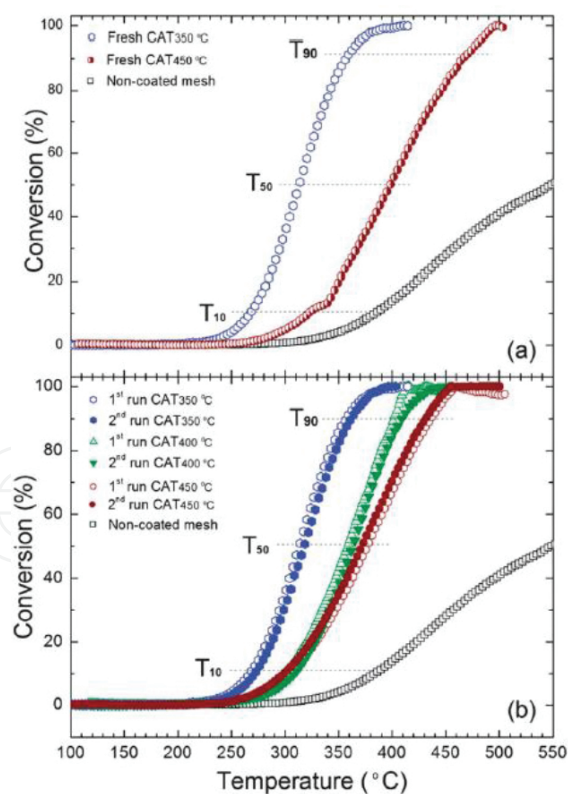
Figure 4. Light-off-curves of C$_3$H$_6$ conversion over a series of α-Fe$_2$O$_3$ coated on the mesh of stainless steel at different temperature and NCM. CAT$_{350}$, CAT$_{400}$ and CAT$_{450}$ represent α-Fe$_2$O$_3$ deposited at 350, 400 and 450°C, respectively. The total flow rate was kept at 15 ml min^{-1} with 1% of C$_3$H$_6$ and 10% of O$_2$ diluted in Ar at the WHSV of 45,000 g$_{cat}^{-1}$ h^{-1}. Reproduced with permission from [54]. Copyright 2013, the Royal Society of Chemistry.

	OL (%)	OH⁻ (%)	O–C=O, C=O (%)	H₂O (%)	Oads/OL	T10 (°C)		T50 (°C)		T90 (°C)	
						FS	PS	FS	PS	FS	PS
CAT350	46.52	25.87	22.76	–	1.05	264	260	326	315	405	350
CAT400	31.19	23.69	41.20	3.92	2.21	–	295	–	355	–	400
CAT450	27.31	25.47	43.82	3.41	2.66	326	302	405	380	470	435

Reproduced with permission from [54]. Copyright 2013, the Royal Society of Chemistry.

Table 1. XPS peak deconvolution result in percentage O_{abs}/O_L ratio, T_{10}, T_{50}, T_{90} of α-Fe$_2$O$_3$ at different deposition temperature.

To identify the phenomenon governing the difference in activity between the three catalysts, a correlation between the catalytic behavior and the α-Fe$_2$O$_3$ characterization results was made [54]. XPS results revealed the presence of both adsorbed and lattice oxygen (**Figure 3B**). The Oadsorbed/Olattice ratio of CAT$_{350}$ was the lowest among the three samples [54]. The catalytic tests over fresh and pretreated samples reveal the negligible role of the adsorbed oxygen, suggesting that the lattice oxygen plays a key role in the reaction sequence. This was corroborated by the TPR experiments, as shown in **Figure 3A**. In addition, it has been observed by Xie et al. [60] and Wang et al. [61] that the morphology or the crystal plane of metal oxides nano-crystal can remarkably alter their catalytic performance. As revealed by the HIM analysis, the film morphology of PSE-CVD made hematite was found to be significantly dependent on the deposition temperature (see **Figure 3C**). The increase of the preparation temperature leads to a variation of film morphology, which is responsible of the increase of the grain size. The grain size is one of the most crucial factors that determine the catalytic performances of catalysts. It is known that the smaller the grain size, the larger the specific surface area. Therefore, it was assumed that CAT$_{350}$ with the smallest grain size and fine crystal structure possesses the largest specific surface area. This argument was consistent with the experimental observation that CAT$_{350}$ presents the best performance.

Based on the TPR, XPS and HIM results, the possible oxidation mechanism of C$_3$H$_6$ over the as-prepared catalysts was suggested to follow a Mars-van Krevelen (MvK) mechanism, an intrafacial mechanism which involves migration of bulk oxygen to the surface, where it participates in the reaction with the reactant and replacement of bulk oxygen by oxygen from the gas phase [62]. Previous investigations have pointed out that this mechanism is valid in the combustion of hydrocarbons over transition metal oxide catalysts [63]. Also, catalytic combustion of C$_3$H$_6$ over Co$_3$O$_4$ has been reported by Liotta et al. [10] to proceed with the MvK mechanism.

3.1.3. Manganese oxides

Considering the low toxicity and availability, manganese oxides have attracted great attention among the various different transition metal oxides. Besides its unique physic-chemical properties, high activity and durability, they were extensively studied as catalysts [64–66]. Manganese oxides possess a wide range of crystal phases (β-MnO$_2$, γ-MnO$_2$, α-Mn$_2$O$_3$,

γ-Mn_2O_3, α-Mn_3O_4 and Mn_5O_8) as well as variable oxidations states (+II, +III, +IV), which confer strong ability to switch from one oxidation state to another one and enable the formation of defects in the lattice, beneficial to the high oxygen mobility and oxygen storage [67]. Catalytic oxidation of VOCs (benzene and toluene) was investigated over a series of manganese oxide catalysts (Mn_3O_4, Mn_2O_3 and MnO_2). The sequence of catalytic activity was found as follows: $Mn_3O_4 > Mn_2O_3 > MnO_2$, which was closely correlated with the oxygen mobility on the catalyst [68]. Following the same logic, an investigation of the role of lattice oxygen in catalytic activity of manganese oxides toward the oxidation of ethanol, ethyl acetate and toluene has been performed by Santos et al. [69]. The results indicate that Mn_3O_4 improves catalytic performance due to the increased reactivity and mobility of lattice oxygen. In a recent paper, Tian et al. [43] have reported that Mn_3O_4 is a highly stable and active catalyst in many respects comparable to conventional catalysts based on noble metals. The catalytic performance was investigated with respect to the total oxidation of CO and C_3H_6 at atmospheric pressure. The full comparison of the reactants and products is given in **Figure 5**. The oxidation of CO over Mn_3O_4 (**Figure 5a$_1$, a$_3$**) becomes observable at 190°C and complete conversion occurs at 343°C with a temperatures shift to 280 and 820°C for an experiment without Mn_3O_4 (**Figure 5b$_1$, b$_3$**). Compared to the CO oxidation over manganese oxides (MnO_x and Mn_2O_3) prepared by precipitation [70], T_{25} was observed at 298°C, which is higher than the value (250°C) obtained with PSE-CVD Mn_3O_4 [43]. Moreover, the temperature at 50% (T_{50}) of CO conversion was observed at 271°C, demonstrating that Mn_3O_4 prepared by PSE-CVD is highly active in the deep oxidation of CO.
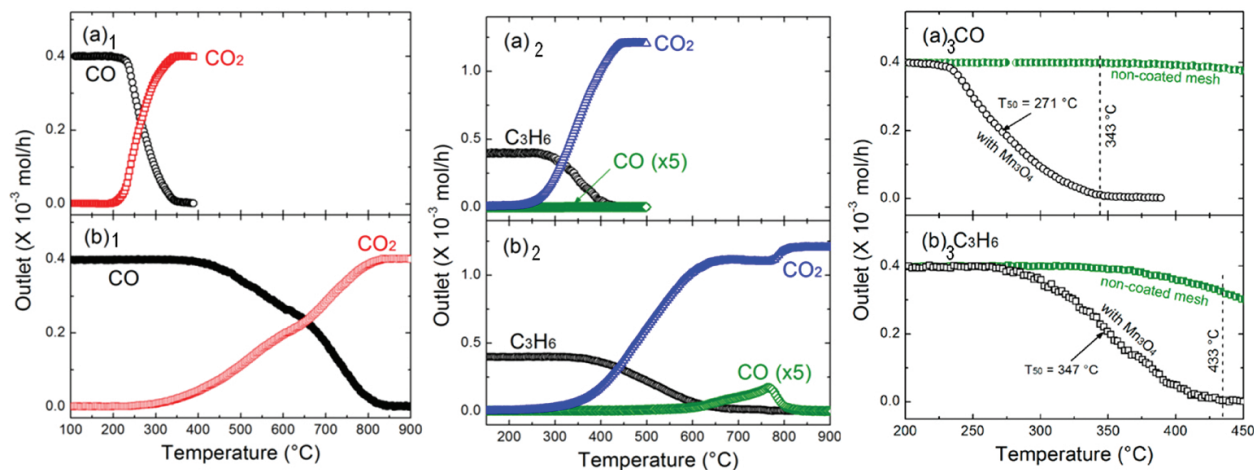

Figure 5. Production and light-off curves of CO and C_3H_6 oxidation over Mn_3O_4-coated mesh (a$_1$, a$_2$ and a$_3$) and NCM (b$_1$, b$_2$ and b$_3$), respectively. Light-off curve of CO (a$_3$) and C_3H_6 (b$_3$) oxidation over Mn_3O_4-coated mesh and NCM. The reaction was carried at the total flow rate was kept at 15 ml min^{-1} with 1% of C_3H_6 and 10% of O_2 diluted in Ar corresponding the WHSV of 45,000 g_{cat}^{-1} h^{-1}. Reproduced with permission from [43]. Copyright 2013, American Chemical Society.

It was also observed that the conversion of C_3H_6 on Mn_3O_4 (**Figure 5, a$_3$**) becomes detectable at 220°C and conversion of C_3H_6 approaches 100% at 433°C. However, the oxidation of C_3H_6 on NCM starts at ~290°C and a temperature as high as 821°C (**Figure 5b$_2$, b$_3$**) was required for complete conversion of C_3H_6. More importantly, at low C_3H_6 conversions, the main product is

CO_2, but a trace of CO peaking at 769°C (**Figure 5b$_2$**) was formed on NCM, which results from partial oxidation. However, except CO_2 and water, no other by-products were detected in the presence of Mn_3O_4, indicating that Mn_3O_4 is effective to reduce CO emission.

The catalytic oxidation of CO and C_3H_6 over Mn_3O_4 was suggested to likely follow the MvK mechanism which involves reversible reduction/reoxidation steps of the lattice oxygen atoms. As reported in the above-mentioned text, trapped oxygen was apparently released with the increase of the temperature and Mn_3O_4 tends to be reduced through the subsurface oxidation of CO or C_3H_6 with the lattice or surface oxygen. Subsequently, the reduced metal oxide site is reoxidized by the atmospheric O_2. According to the redox results [43], Mn_3O_4 was easier to be reoxidized than to be reduced, demonstrating that the reduction step could play a crucial role in the kinetics of the catalytic oxidation process. The abundance of adsorbed oxygen, revealed in the XPS results in addition to the excellent redox behavior [43], can play a key role in the oxidation process.

3.1.4. Copper oxide

Copper oxide is a promising semiconductor material which is widely exploited for a broad field of applications. As CuO is nontoxic and its constituents are abundantly available, the synthesis of CuO is considered as an important research topic for catalytic processes. Copper oxide is unique as it has square planar coordination of copper by oxygen in the monoclinic structure. TMOs, such as Co_3O_4 and Mn_3O_4, are effective catalysts for the oxidative destruction of VOCs [24]. However, not much is known concerning the abatement of CO and VOCs with CuO [71–73]. The selective oxidation of propene with O_2 to propylene oxide and acrolein has been study by Hua et al. [74] and the results indicate that Cu_2O nanocrystals control the catalytic selectivity as well as the activity in propylene oxidation with O_2. In addition, the authors also reveal the underlying structure-activity relationships of this complex heterogeneous catalytic reaction at the molecular level and identify the catalytically active sites. Most recently, Tian et al. [44] and Pan et al. [45] have studied the low-temperature complete oxidation of VOCs of olefins type such as C_2H_2 and C_3H_6 over CuO_x. They have demonstrated that CuO and Cu_2O are active and promising catalyst for the abatement of VOCs.

The catalytic performance of the CuO was evaluated for the complete oxidation of C_3H_6 by Tian et al. [44]. The background effect of the mesh on the combustion process was examined by carrying out the oxidation of C_3H_6 on NCM under the same gas inlet conditions. **Figure 6** compares the conversion temperature of C_3H_6 production over CuO films and NCM. The conversion plots show clearly that CuO favors the total oxidation C_3H_6 (**Figure 6a**) at lower temperatures relative to NCM. In the presence of CuO, the consumption of C_3H_6 was observable at about 190°C and complete conversion was reached within 310°C, while these two values shift toward higher temperatures for the reaction on NCM. No trace of CO was detected in the oxidation process with CuO (**Figure 6b**). However, a significant amount of CO was formed in the reaction without catalyst, which was assigned to come from the partial oxidation reaction. In the two cases, CO_2 was observed to be the final product. The temperatures *T10*, *T50,* and *T90*, corresponding to the 10, 50 and 90% C_3H_6 conversion during the temperature-programmed reaction, were selected to compare the catalytic performance of the deposited CuO as well

as some representative catalysts available in the literature (see **Table 2** in Section 2.1.6) toward C_3H_6 oxidation.
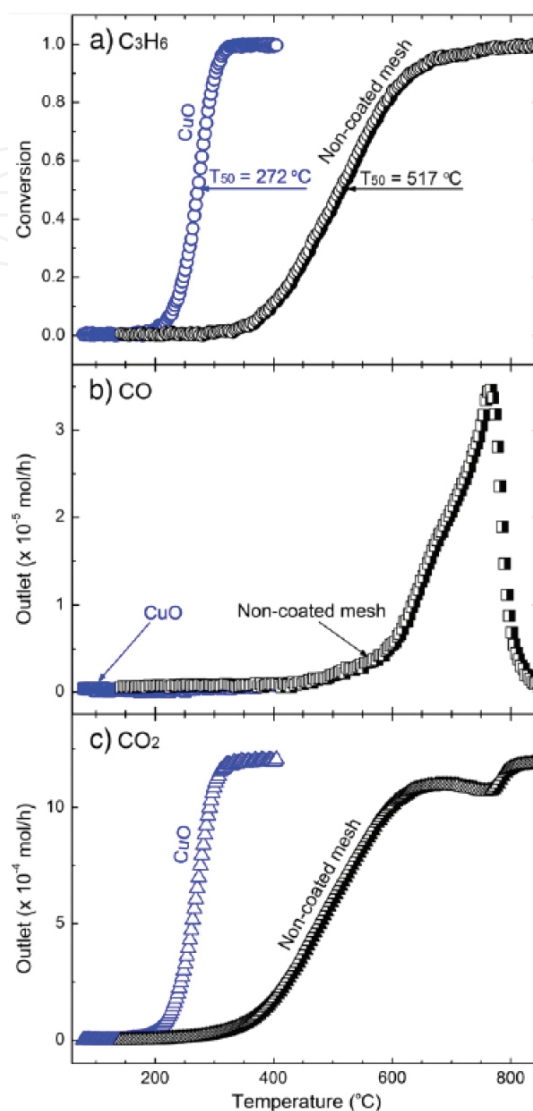

Figure 6. Light-off curves for C_3H_6 oxidation: conversion of C_3H_6 (a); associated CO production (b) and CO_2 production (c) with CuO-coated and NCM. The reaction was carried at the total flow rate was kept at 15 ml min^{-1} with 1% of C_3H_6 and 10% of O_2 diluted in Ar corresponding the WHSV of 45,000 g_{cat}^{-1} h^{-1}. Reproduced with permission from [44]. Copyright 2013, Elsevier.

Cu_2O was also tested by Pan et al. [45] as catalyst for the deep oxidation C_2H_2 and C_3H_6. The catalytic tests were carried out three times for the same sample and the results were quite close, demonstrating that the prepared Cu_2O has good reusability with reproduced results. **Figure 7A** compares the temperature-dependent conversion ratio of C_2H_2 and C_3H_6 with Cu_2O-coated mesh and NCM. Compared to the NCM condition, the complete oxidation of C_2H_2 decreased from 450 to 300°C and for C_3H_6 decreased from 675 to 425°C over Cu_2O. It should be mentioned that during the oxidation of C_2H_2 and C_3H_6 over Cu_2O-coated mesh, CO was not detected. However, CO was detected abundantly over NCM. Compared to oth-

er TMOs such as Mn_3O_4 [43] and Co_3O_4 [23] for the oxidation of C_2H_2 and C_3H_6, Cu_2O exhibits much better catalytic performances. With an Arrhenius expression, apparent activation energies (E_a) of <15% of C_2H_2 and C_3H_6 conversion were deduced. The E_a of C_2H_2 and C_3H_6 oxidation over NCM was 93.5 and 92.0 kJ mol^{-1}, while these values shift to 51.7 and 57.0 kJ mol^{-1} with Cu_2O-coated samples (average values for three times), respectively. Compared to E_a obtained with other TMOs, such as Co_3O_4 (128.9 kJ mol^{-1} for C_2H_2, 127.1 kJ mol^{-1} for C_3H_6) [48] and Mn_3O_4 (84.7 kJ mol^{-1} for C_3H_6) [43], the reaction with Cu_2O also shows lower E_a. Thus, the relatively low E_a was suggested to contribute in the acceleration of the oxidation processes and enhances the catalytic performance for the oxidation of C_2H_2 and C_3H_6. As redox mechanism is generally accepted to be the dominant mechanism in the oxidation of low-rank hydrocarbons over TMOs, both authors also suggested CuO and Cu_2O follow a redox process. According to Pan et al. [45], Cu_2O is suggested to react first with oxygen, giving rise to CuO. Second, the reaction of C_2H_2 and C_3H_6 with the trapped or lattice oxygen occurs, leading to CuO reduction and release of oxygen to form Cu_2O. From the XPS results (**Figure 7B**), O 1s core shell shows mainly O_2^{2-} and O^- species. Both O_2^{2-} and O^- are known as strongly electrophilic reactants capable to attack an organic molecule in the region of its highest electron density and result in the oxidation of the carbon skeleton. As the electrophilic oxygen species such as lattice and adsorbed oxygen generally participates in the total oxidation of hydrocarbons to CO_2, these electrophilic oxygen species (O_2^{2-} or O^-) presented at the surface of Cu_2O were suggested to be also benefit for the complete conversion of C_2H_2 and C_3H_6.
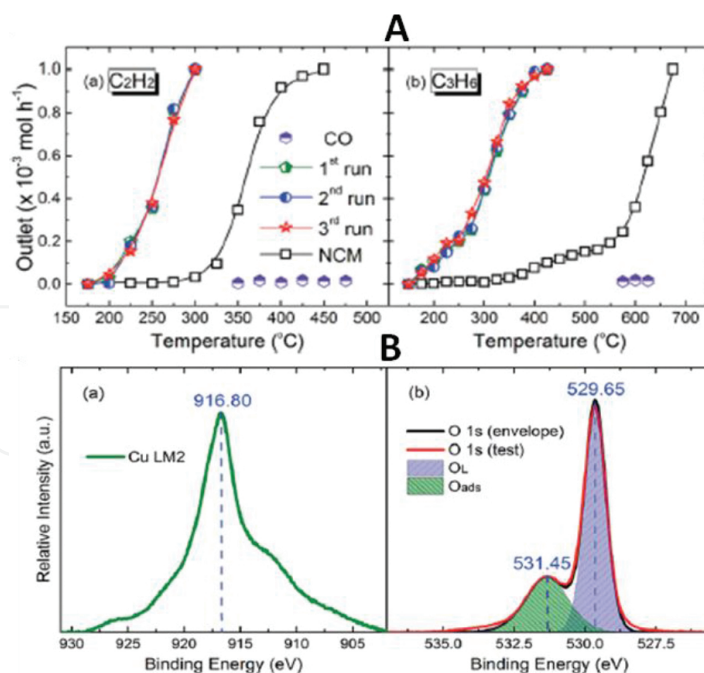

Figure 7. Outlet profiles of C_2H_2 A (a) and C_3H_6 A (b) oxidation over NCM and mesh grid of stainless steel coated with Cu_2O. The reaction was carried at the total flow rate was kept at 15 ml min^{-1} with 1% of fuel and 10% O_2 diluted in Ar, corresponding the WHSV of 45,000 g_{cat}^{-1} h^{-1}. Cu LM2 B (a) and O 1s signals B (b) of representative Cu_2O thin film. Reproduced with permission from [45]. Copyright 2015, the Royal Society of Chemistry.

3.1.5. Chromium oxide

Chromium oxide (Cr_2O_3) has been broadly and successfully used for numerous applications such as wear resistance, corrosion protection, optics and electronics due to its high melting point, heat resistance, mechanical strength, chemical inertness, optical characteristics, high hardness and low friction coefficient [75–79]. It has been proved to be active when used as catalyst for the destruction of halogenated compounds. In addition to its good thermal stability, Cr_2O_3 exhibited attractive performance in the low-temperature abatement of VOCs. Recently, Liang et al. [46] reported the synthesis of Cr_2O_3 by PSE-CVD for the total oxidation of propene. **Figure 8** compares the temperature-dependent conversion of C_3H_6 to CO_2 as the final product and the associated CO production over Cr_2O_3 films and NCM. The conversion plots show clearly that Cr_2O_3 enables the oxidation of C_3H_6 at lower temperatures relative to the NCM. In the presence of Cr_2O_3, the consumption of C_3H_6 becomes observable at about 400°C and complete conversion occurs around 550°C, while these temperatures were observed to shift, respectively, to 600 and 775°C for the reaction on NCM. Compared to the T_{50} of C_3H_6 conversion, T_{50} obtained with Cr_2O_3 was quite close to the values reported for Au/Al_2O_3 and $La_{1.7}Sr_{0.3}CuO_4S_{0.2}$, which indicates that the PSE-CVD made Cr_2O_3 exhibits similar catalytic performance to the noble metal and perovskite. During the oxidation of C_3H_6 over Cr_2O_3-coated mesh, only a small amount of CO was detected. However, considerable quantities of CO (**Figure 8b**) were formed in the reaction without catalyst, which could originate from the partial oxidation reaction.
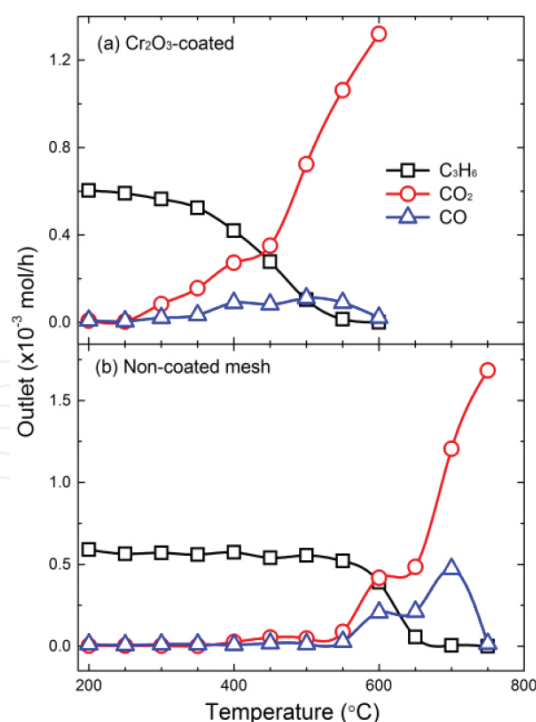

Figure 8. Outlet profiles of C_3H_6 oxidation over Cr_2O_3-coated and NCM. The reaction was carried at the total flow rate was kept at 15 ml min^{-1} with 1% of fuel and 10% O_2 diluted in Ar, corresponding the WHSV of 62,500 g_{cat}^{-1} h^{-1}. Reproduced with permission from [46]. Copyright 2015, Wiley-VCH.

Diffuse reflectance infrared Fourier transformed spectroscopy (DRIFTS) was used to study the possible catalytic reaction mechanism of Cr_2O_3. A feed of argon gas containing 1% of C_3H_6 and 10% of O_2 was introduced into the reactor which was equipped with a small piece of stainless steel grid mesh as the catalyst support. The IR spectra at different temperatures are presented in **Figure 9**. Surface adsorption species with IR bands at 729 and 913 cm⁻¹ are clearly observed at temperature lower than 100°C, which were assigned to adsorption of C_3H_6 on the deposited film. These bands were still detectable below 300°C. When the temperature increases to 500°C, the coordinated C_3H_6 vanishes gradually and CO_2 was detected. The temperature for the complete conversion of C_3H_6 to CO_2 was around 500°C, in good agreement with the catalytic tests.
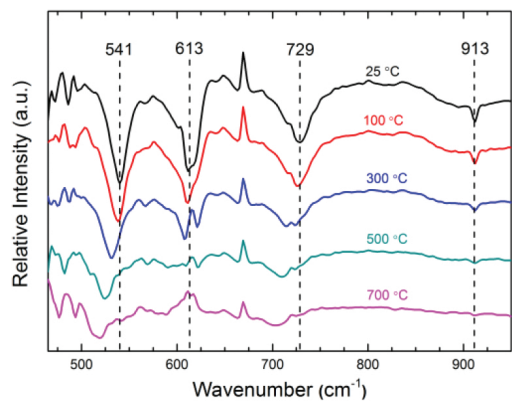

Figure 9. In-situ DRIFTS spectra of Cr_2O_3 during C_3H_6 adsorption at different temperatures. Reproduced with permission from [46]. Copyright 2015, Wiley-VCH.

3.1.6. Comparison of the catalytic performances of single TMOs with literature

Table 2 summarizes and compares the catalytic performance of the PSE-CVD made single TMOs with that of the selected catalysts in the literature. Even though the experimental condition was not exactly the same, regarding the weight of the catalyst and the WHSV, our catalysts present comparable activity to the systems presented in the table. Special attention is paid to the comparison of the catalytic performance with noble metals and transition metal oxides. As it can be seen from **Table 2**, noble metals and TMOs (single) present attractive results in terms of CO and propene total oxidation.

Type of catalyst	Material	Weight (mg)	Gas composition	WHSV [a] (ml g⁻¹ h⁻¹)	T_{10} [b] (°C)	T_{50} [b] (°C)	T_{90} [b] (°C)	Refs.
Single TMOs	α-Fe_2O_3	20	1% C_3H_6/10% O_2 in Ar	45,000	260	313	350	[54]
	α-Fe_2O_3 400°C				295	355	400	
	α-Fe_2O_3 450°C				302	380	435	
	Co_3O_4	12	1% C_3H_6/10% O_2 in Ar	75,000	306	347	396	[23]

Type of catalyst	Material	Weight (mg)	Gas composition	WHSV ^{a} (ml g^{-1} h^{-1})	T$_{10}$ ^{b} (°C)	T$_{50}$ ^{b} (°C)	T$_{90}$ ^{b} (°C)	Refs.
	Co$_3$O$_4$	41.5	2% C$_3$H$_6$/20%O$_2$ in Ar	73,000	293	327	356	[48]
	Co$_3$O$_4$	12		75,000	325	354	385	[24]
	CuO	12	1% C$_3$H$_6$/10% O$_2$ in Ar		–	272	–	[44]
	Cu$_2$O	20		45,000	–	300	–	[45]
	Cr$_2$O$_3$	10			–		–	[46]
	Mn$_3$O$_4$	12		75,000		347		
Precious metal	Au/Al$_2$O$_3$	200	1.5% C$_3$H$_6$/4% O$_2$ He	22,500	288	349	410	[80]
	Au/Al$_2$O$_3$		1% C$_3$H$_6$/9% O$_2$ in He	219,512	–	365	–	[91]
	Au/BaO/Al$_2$O$_3$			250,000	–	290	–	
	Au/Rb$_2$O/Al$_2$O$_3$			257,143	–	307	–	
	Au/Li$_2$O/Al$_2$O$_3$			225,000	–	327	–	
	Au/MgO/Al$_2$O$_3$			214,286	–	359	–	
	Ag/Al$_2$O$_3$	50	3% C$_3$H$_6$/10% O$_2$ in N$_2$	12,000	–	–	420	[95]
Single TMOs	α-Fe$_2$O$_3$ thin film	20	1% CO/10% O$_2$/89% Ar	45,000	–	319	364	[25]
	Fe$_2$O$_3$	50	3.44% CO/20.6 O$_2$% in He	1,200,000	–	300	330	[96]
	Fe$_2$O$_3$	1000	2.5% CO/1.7% O$_2$/0.5% H$_2$ in He	60,000	–	367	397	[53]
	Fe$_2$O$_3$/TiO$_2$				–	333	412	
	Fe$_2$O$_3$/Al$_2$O$_3$		2.5% CO/1.7% O$_2$/0.5% H$_2$/He		–	327	377	
	Co$_3$O$_4$ thin film	12	1% CO/10% O$_2$/89% Ar	75,000	–	335	350	[23]
	Co$_3$O$_4$ bulk	50	1% CO/8% O$_2$ in He	44,400	–	–	350	[90]
	Co$_3$O$_4$ thin film	12	1% CO/10% O$_2$ in Ar	75,000	306	347	396	[23]
	CeO$_2$	100	2% CO/2% O$_2$ in N$_2$	60,000	–	–	374	[97]
	Al$_2$O$_3$	100	2% CO/2% O$_2$ in N$_2$		–	–	394	
	Mn$_3$O$_4$	12	1% CO/10% O$_2$ in Ar	75,000	–	271		[43]
Precious metals	Pt/H$_2$SO$_4$/ZrO$_2$	50	3.5% CO/4% O$_2$ in N$_2$	120,000	–	–	290	[98]
	Pt/Al$_2$O$_3$	2/200	1% CO/1.38% O$_2$ in N$_2$	90,000	–	333	430	[89]
	Au/SiO$_2$	100	1% CO/99% dry air	12,000	–	337	423	[99]

^{a}: *Weight hourly space velocity*
^{b}: *Temperature at X% conversion (X=10, 50 and 90 %)*

Table 2. Overview of the catalytic performances of PSE-CVD single made TMOs compared with the literature.

3.2. CO and VOCs oxidation over PSE-CVD made binary TMOs catalysts

Among the different mixed-oxide structures, numerous references can be found, dealing with the reactivity of perovskites such as compounds with A_2BO_4 structure or spinel-type mixed oxide (AB_2O_3) for the CO and VOCs oxidation reaction. Since the 1970s, some spinel-type mixed oxides are known to exhibit activity for CO and VOCs oxidation. In order to further improve the catalytic performance of TMOs, some combinations of oxides have been formulated and the obtained binary or mixed TMOs have exhibited better activities than the single or mixed components or even comparable with that of noble metals. Such catalysts include Co-Mn [24], Cu-Co [28] and Co-Fe [25–27]. It is important to note that, because of the weak performances of Cr_2O_3 catalyst compared to other single oxide presented in this review, in addition to highly toxicity, we have restricted the application of Cr-based catalysts to low operation temperatures.

3.2.1. Catalytic oxidation of VOCs over mixed Co-Mn oxides made by PSE-CVD

Tian et al. have studied the catalytic oxidation of VOCs over spinels $Co_{3-x}Mn_xO_4$ ($0 \leq x \leq 0.34$) binary oxides obtained by PSE-CVD. The grown Co-Mn binary oxides were tested toward the total oxidation of C_2H_2 and C_3H_6 as illustrative examples [24]. The TPR/TPO results and the light-off curves of the samples are presented in **Figures 10** and **11** and summarized in **Table 3**. **Figure 10A** compares the temperature-dependent conversion of C_2H_2 and C_3H_6 over $Co_{3-x}Mn_xO_4$ films and NCM. The detailed outlet profiles of the fuels and products are given in **Figure 11**. The temperatures T_{50}, T_{90}, T_{50}, and T_{90} of CO_2, corresponding to the temperatures of CO_2 production, were selected as parameters to indicate the catalytic activity of the deposited samples toward the deep oxidation of hydrocarbons, as shown in **Table 3**. The catalytic performances were improved from Co_3O_4 to $Co_{2.66}Mn_{0.34}O_4$, both being superior to the NCM.
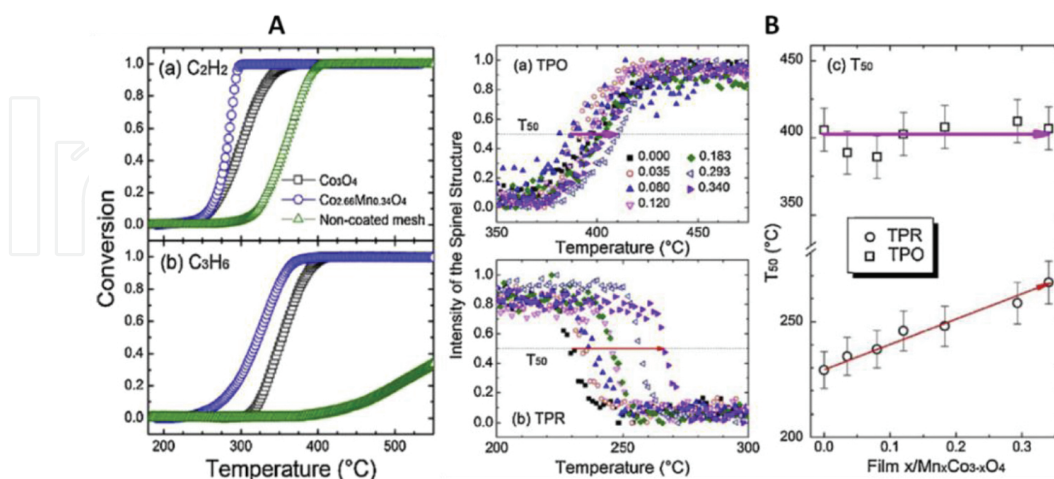

Figure 10. (A) Light-off curves of C_2H_2 and C_3H_6 over $Co_{3-x}Mn_xO_4$ ($x = 0$ and 0.34) spinel structures grown on mesh of stainless steel substrates and NCM. The reaction was carried at the total flow rate was kept at 15 ml min^{-1} with 2% of fuel and 20% O_2 diluted in Ar at a total flow rate of 0.015 L/min; (B) TPO/TPR patterns of Co-Mn oxide. Reproduced with permission from [45]. Copyright 2015, Elsevier.
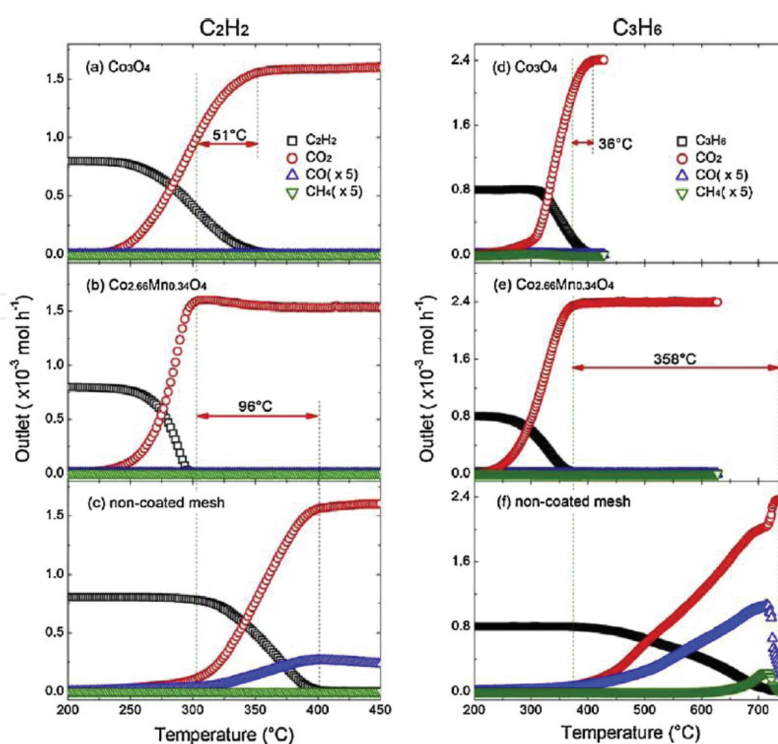
Figure 11. Production profiles of C_2H_2/C_3H_6, CO, CO_2 and CH_4 in the oxidation of C_2H_2 and C_3H_6 over $Co_{3-x}Mn_xO_4$ oxides (x = 0 and 0.34) grown on mesh of stainless steel substrates and NCM. Reproduced with permission from [24]. Copyright 2015, Elsevier.

Fuel	Catalyst	T_{50} (°C)[a]	T_{90} (°C)[a]	T_{50} CO_2 (°C)[b]	T_{90} CO_2(°C)[b]	Ea (kJ mol^{-1})[c]
C_2H_2	NCM	355	386	356	387	168.97
	Co_3O_4	299	335	301	337	139.77
	$Co_{2.66}Mn_{0.34}O_4$	282	294	282	295	131.86
C_3H_6	NCM	603	692	614	723	121.98
	Co_3O_4	354	385	356	387	158.32
	$Co_{2.66}Mn_{0.34}O_4$	321	356	323	357	114.59

Reproduced with permission from [24]. Copyright 2012, Elsevier.

[a]T_{50} and T_{90} represent the temperatures at which the conversion of C_2H_2/C_3H_6 reaches 50 and 90%, respectively.

[b]T_{50} CO_2 and T_{90} CO_2 represent the temperatures at which 50 and 90% conversion to CO_2 is reached.

[c]Ea is the apparent activation energy for the hydrocarbon activation at atmospheric pressure.

Table 3. Catalytic oxidation of C_2H_2/C_3H_6 over Co-Mn oxides catalysts deposited on grid mesh of stainless steel substrates and NCM.

The selectivity-conversion plots show clearly that the investigated coatings favor the total oxidation of both unsaturated hydrocarbons at lower temperatures relative to the NCM. For

C_2H_2, T_{50} and T_{90} were observed at 355 and 386°C over NCM, whereas these values decreased by respective 56 and 51°C over cobalt oxide and further decreased by 17 and 41°C over $Co_{2.66}Mn_{0.34}O_4$, which reveals that the catalyst with small amount of manganese content shows the highest activity (see **Figure 10** and **Table 3**). Tian et al. [48] reported that T_{50} of C_2H_2 oxidation with Co_3O_4 deposited on monolithic cordierite support was 297°C, which was in good agreement with the current Co_3O_4 sample prepared on mesh. Note that the T_{50} of C_2H_2 (282°C, **Table 3**) with $Co_{2.66}Mn_{0.34}O_4$ [24] was quite close to the value (280°C) reported by Ivanova et al. [80] who used Au/Al_2O_3, revealing that $Co_{2.66}Mn_{0.34}O_4$ prepared by CVD features a competitive activity. The low-temperature shift of the light-off curve was more pronounced for C_3H_6 since the T_{90} difference between the NCM and $Co_{2.66}Mn_{0.34}O_4$ is 336°C, demonstrating that $Co_{2.66}Mn_{0.34}O_4$ was very active for the total oxidation of propene and supporting the conclusion of Liang et al. [81] who reported that the manganese insertion into the cobalt oxide spinel could enhance the catalytic activity of the oxidation of light olefins. Considering the higher activity, Mn-doped spinel of cobalt oxide could be a potential system for catalytic oxidation of hydrocarbons. As presented in **Table 3**, the values of T_{50} and T_{90} of hydrocarbons conversion and those of CO_2 selectivity were found to be almost identical for Co_3O_4. However, differences were observed relative to NCM especially in the oxidation of C_3H_6, illustrating an occurrence of partial oxidation by generating products other than CO_2 (see **Figure 11f**). With Co_3O_4 and $Co_{2.66}Mn_{0.34}O_4$, CO_2 was observed to be the only carbonaceous product and no secondary products were formed all over the entire oxidation process of C_3H_6, while CO and CH_4, coming from incomplete oxidation, were detected in addition to the production of CO_2 on NCM. Even though some by-products were formed at certain temperatures with NCM, all indicate that CO_2 was the final product. Taking the temperature at which hydrocarbons were completely converted to CO_2 on $Co_{2.66}Mn_{0.34}O_4$ sample as a reference, Co_3O_4 and NCM show a respective increase of 51 and 96°C for C_2H_2 and 36 and 358°C for C_3H_6, which indicate that the use of cobalt together with manganese significantly affects the catalytic activity. By applying the Arrhenius equation in the conversion range within 15% [48], the Ea was calculated (see **Table 3**). In general, the manganese-doped cobalt oxide exhibits lower Ea. Compared to those activation energies obtained in the oxidation of C_2H_2 and C_3H_6 over Co_3O_4-coated monolith with a large flow rate (500 sccm) [48], the values obtained on Co_3O_4-coated mesh were about 10 and 30 kJ mol^{-1} larger, the difference of which may come from the comprehensive effect of the support and inlet condition. Zhang et al. [82] and Aguilera et al. [83] also reported that the modification of Co_3O_4 by MnO_x could promote the preferential oxidation of CO, toluene and alcohols at lower temperatures. The catalytic oxidation of the two hydrocarbons employing Co-Mn oxides systems consists of two irreversible steps, namely the reaction of the hydrocarbon with the lattice or trapped oxygen leading to its reduction and release of oxygen from the surface of the metal oxide and the reoxidation of the partly reduced metal oxide site by means of oxygen in a subsequent step. The TPO analysis indicates that the manganese introduction does not really influence the bulk reoxidation behavior of Co-Mn oxides [24]. Considering the TPR (**Figure 10B**) and catalytic results which reveal that Co_3O_4 has higher reducibility but lower activity than $Co_{2.66}Mn_{0.34}O_4$, the formation of oxygen vacant site plays a key role in the redox mechanism, the importance of which was pointed out previously by Noller and Vinek [84]. According to the enhancement of the thermal stability,

the amount of oxygen vacancy was increased upon manganese incorporation, which accelerates the oxidation process. Furthermore, the catalytic activity could also benefit from the substitution of cobalt with manganese that was more active and from the cooperative effect among metallic species by increasing the oxide reduction sites.

3.2.2. PSE-CVD made cobalt ferrite for low-temperature oxidation of CO and VOCs

Thin films of cobalt ferrite binary oxides (with the general formula $Co_{3-x}Fe_xO_4$) at different composition ($Co_{0.9}Fe_{2.1}O_4$, $Co_{1.8}Fe_{1.2}O_4$ and $Co_{2.1}Fe_{0.9}O_4$) were prepared by PSE-CVD. The systematic characterization of their properties and their potential application as catalysts for low-temperature CO, C_3H_6, n-C_4H_8 and C_2H_6O oxidation has been reported by Kouotou et al. and Tian et al. [27] The effect of iron substitution by cobalt in the structure on the optical and redox properties was investigated. The catalytic performance of the Co-Fe oxides was discussed with respect to the participation of surface and lattice oxygen in the oxidation process. According to XPS and temperature-programmed reduction/oxidation (TPR/TPO) results, a suprafacial mechanism was the dominant mechanism for CO oxidation to CO_2, while C_3H_6, n-C_4H_8 and C_2H_6O were oxidized through an intrafacial process (MvK mechanism).
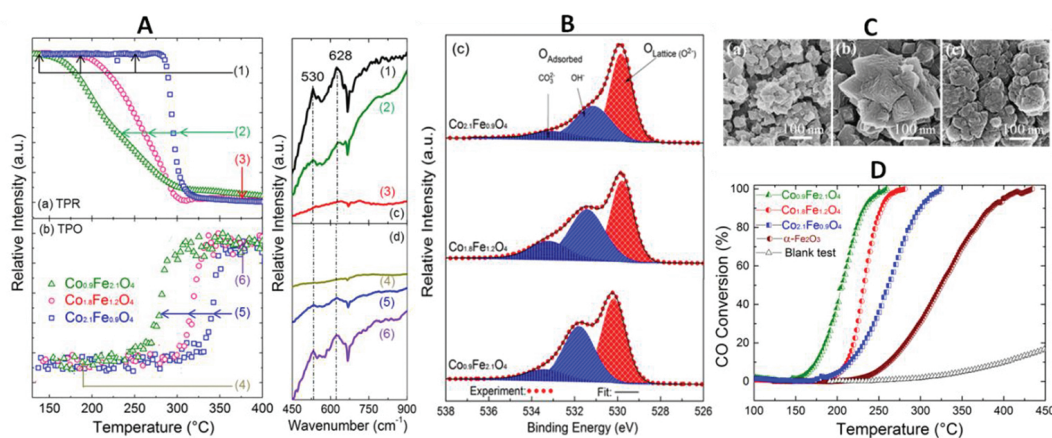

Figure 12. (A) Redox behaviors of Co-Fe oxides: (a) TPR, (b) TPO, (c) progressive loss of the spinel structure and (d) recover of Co-Fe-O IR vibration; (B) O1s XPS spectra of the Co-Fe-O samples; (C) HIM image displaying films morphology; (D) light-off curves of CO conversion with the Co-Fe-O samples, αFe_2O_3 and NCM. The results obtained over αFe_2O_3 [55]. The reaction was carried at the total flow rate was kept at 15 ml min^{-1} with 1% of CO and 10% of O_2 diluted in Ar, corresponding the WHSV of 45,000 g_{cat}^{-1} h^{-1}. Reproduced with permission from [25]. Copyright 2014, the Royal Society of Chemistry.

CO oxidation was performed at atmospheric pressure over all samples. The results were compared with those obtained with pure α-Fe_2O_3 [55] and a blank sample of NCM, as shown in **Figure 12D**. Single α-Fe_2O_3 becomes active in CO oxidation at around 230°C and achieves complete CO conversion to CO_2 above 400°C. Co-Fe-O composites exhibit lower temperatures for the initiation of CO oxidation than the single α-Fe_2O_3. The complete CO oxidation over $Co_{0.9}Fe_{2.1}O_4$, $Co_{1.8}Fe_{1.2}O_4$ and $Co_{2.1}Fe_{0.9}O_4$ occurs at 255, 275 and 325°C, respectively. The results indicate that cobalt ferrites were more catalytically active than single α-Fe_2O_3. The obtained performance order was the following: α-$Fe_2O_3 < Co_{2.1}Fe_{0.9}O_4 < Co_{1.8}Fe_{1.2}O_4 < Co_{0.9}Fe_{2.1}O_4$. It was

observed that the catalytic performance was decreased with the increase of the Co content in the matrix of Co-Fe-O [25]. The sample with low Co content ($Co_{0.9}Fe_{2.1}O_4$) exhibits the highest catalytic performance. An attempt to explain such behavior was made with respect to the difference in the film morphology, redox property and the chemical composition as well as the ionic state at the surface of the material as clearly displayed in **Figure 12** [25].

The TPR and TPO result shows that Co-Fe-O samples were reduced at higher temperature, increasing the Co content (**Figure 12A**). Generally, Co_3O_4, Co^{2+}-Co^{3+} ion pairs are known to be very active in low-temperature CO oxidation [22]. Therefore, the presence in Co-Fe-O composites of both Co^{2+} and Co^{3+} together with Fe^{3+} in the octahedral and tetrahedral sites should enable a decrease of the reduction temperature and an improvement of the catalytic performance of CO conversion to CO_2 over samples with higher Co content ($Co_{2.1}Fe_{0.9}O_4$ and $Co_{1.8}Fe_{1.2}O_4$), which own the $[Co^{2+}Fe^{3+}Co^{3+}]_{O\text{-site}}O_4$ cationic distribution in the O-site. Surprisingly, the opposite behavior was observed with $Co_{0.9}Fe_{2.1}O_4$ (the most active sample) in which only Fe^{3+} and Co^{2+} were present in the octahedral sites ($[Fe^{3+}Co^{2+}]_{O\text{-site}}O_4$). It was thus suggested that the CO oxidation over Co-Fe-O catalyst does not proceed with the redox mechanism, even if $Co_{0.9}Fe_{2.1}O_4$ presents the lowest reduction temperature (**Figure 12A**). The redox mechanism hypothesis was strongly supported by the fact that CO oxidation of $Co_{2.1}Fe_{0.9}O_4$ was initiated at ~200°C while the reduction started at ~280°C (**Figure 12A, D**). Since the formation of carbonates on the cobalt surface has been suggested by Thormählen et al. to play an important role in the low-temperature oxidation of CO [85], the earlier initiation of the reaction at low temperature was therefore assigned to the surface-adsorbed oxygen revealed by XPS analysis (**Figure 12B**). It was thus proposed that CO oxidation over Co-Fe-O follows a suprafacial mechanism where CO molecules react with adsorbed oxygen, mainly as Co_3^{2-} and OH^-, giving rise to form CO_2.

In order to study further the catalytic activity of cobalt ferrite thin films, Tian et al. have investigated the catalytic performance of cobalt ferrite ($Co_{2.1}Fe_{0.9}O_4$) with respect to the total oxidation of propene, n-butene and DME at atmospheric pressure referring to NCM [27]. The catalytic effect of the mesh has been excluded by the observation that there is no significant difference between the oxidation over NCM and in a blank system (**Figure 13**). The results show that the cobalt ferrite films favor the complete conversion of the reactants at much lower temperatures relative to NCM. Besides the reactant gas, CO_2 was detected as the unique product in the oxidation processes over cobalt ferrite, while additional CO was observed in the reaction on NCM. T_{50} and T_{90}, corresponding to respective 50 and 90% conversion of the reactant gas, were used as parameters to compare the performance of the deposited samples. With cobalt ferrite, T_{50} and T_{90} of propene oxidation were 348 and 382°C. These values shifted to 578 and 691°C for the experiment carried out with NCM (see **Figure 13a, b**), respectively. Compared to the reaction over Co_3O_4 with Ea of 158.32 kJ/mol [24], the introduction of iron tends to initiate the oxidation of propene with lower Ea, which makes the cobalt ferrite more suitable for the catalytic applications. **Figure 13c** and **d** compares the results of n-C_4H_8 oxidation with and without cobalt ferrite. T_{50} and T_{90} of n-C_4H_8 oxidation over cobalt ferrite were observed at 358 and 402°C, whereas these values shifted by respective 100 and 135°C toward higher temperatures over NCM. It has been reported that a small quantity of 1,3-

butadiene was selectively formed in the oxidation of n-C_4H_8 at temperature higher than 350°C over MnMoO$_4$-based catalysts [86]. It should be noted that 1,3-butadiene was not detected in the reaction with the PSE-CVD made $Co_{2.1}Fe_{0.9}O_4$ indicating that the material presents higher catalytic activity.
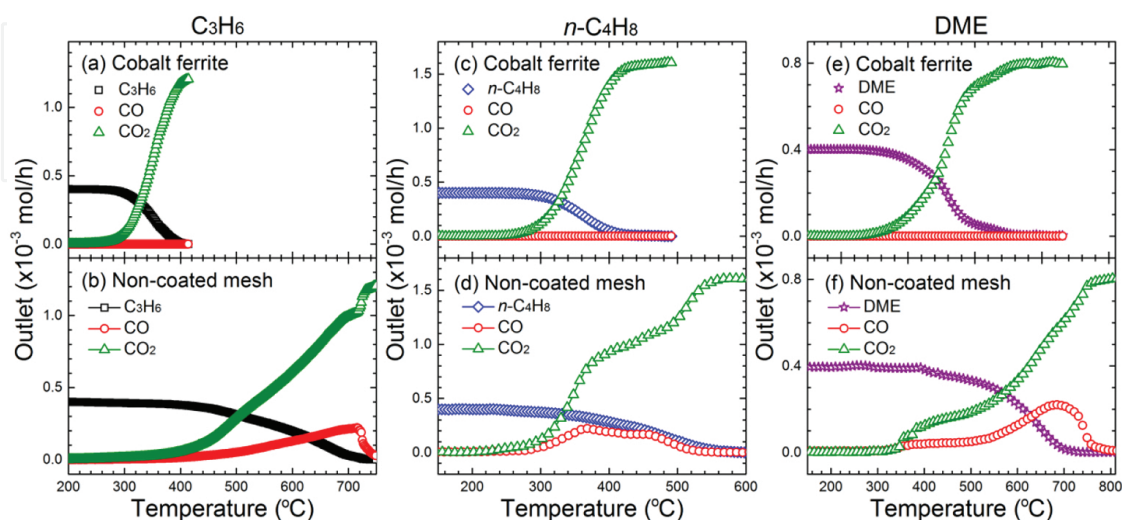

Figure 13. Outlet profiles of C_3H_6, n-C_4H_8 and DME oxidation over cobalt ferrite-coated and non-coated meshes. The reaction was carried at the total flow rate was kept at 15 ml min^{-1} with 1% of Fuel and 10% of O$_2$ diluted in Ar, corresponding the WHSV of 45,000 g$_{cat}$$^{-1}$ h^{-1}. Reproduced with permission from [27]. Copyright 2015, Elsevier.

For DME, cobalt ferrite also exhibits much better performance than NCM, as revealed in **Figure 13e** and **f**. T_{50} and T_{90} of the reaction over cobalt ferrite are 356 and 409°C. These values were observed to be 613 and 682°C for the reaction on NCM, respectively. According to Liu et al. [87], the reaction network for DME conversion contains four pathways giving rise to CH_3OH, $HCHO$, $HCOOCH_3$ and CO_x. Low selectivity of CH_3OH and $HCOOCH_3$ was reported [87]. HCHO was not detected, which could be resulted either from the low concentration or fast conversion to CO_x.

The good catalytic performance of cobalt ferrite could be correlated with the O$_{adsorbed}$ on the surface and attractive redox properties (**Figure 12A, B**). It is widely accepted that the catalytic performance of ferrite-type catalysts depends on its oxygen mobility since the reaction follows MvK mechanism [88]. The abundance of O$_{Adsorbed}$ could participate in the catalytic oxidation process, as proposed by Veleva and Trifirò [86]. The good reducibility and reoxidability tend to enable the catalytic reactions at relatively low temperatures by involving various cations distributed in the octahedral and tetrahedral sites. Moreover, the slightly low band gap energy of cobalt ferrite could also indicate that the migration of O$_{lattice}$ or O^{2-} from the bulk to the surface becomes easier and leads to good reducibility [25].

Because cobalt ferrite binary oxide with high Co concentration ($Co_{2.1}Fe_{0.9}O_4$) showed very interesting catalytic performance against the deep oxidation of C_3H_6, n-C_4H_8 and DME, Kouotou et al. [26] explored the catalytic activity of the same material, but with low Co concentration ($CoFe_2O_4$). Authors aimed to compare the performances of $CoFe_2O_4$ (low cobalt

content) versus $Co_{2.1}Fe_{0.9}O_4$ (high cobalt content) from recent investigation toward catalytic oxidation of CO, DME, C_3H_6 and n-C_4H_8. The role of Co or Fe atom in the matrix of cobalt ferrite mixed oxide and adsorbed/lattice oxygen at the surface of the deposited material in the catalytic reaction was identified. The light-off curves of CO, C_3H_6, n-C_4H_8 and DME oxidation over $CoFe_2O_4$ are shown in **Figure 14**. The results indicate that $CoFe_2O_4$ is a very active catalyst for the total oxidation of CO, C_3H_6, n-C_4H_8 and DME at atmospheric pressure. Total destruction of such pollutants at low temperature enables the production of CO_2 as the only detectable C-containing product. In the presence of $CoFe_2O_4$, the oxidation becomes detectable at around 150, 200, 230 and 270°C for CO, C_3H_6, n-C_4H_8 and DME, respectively and complete conversion occurs at 253°C for CO, 336°C for C_3H_6 and n-C_4H_8 and 502°C for DME.
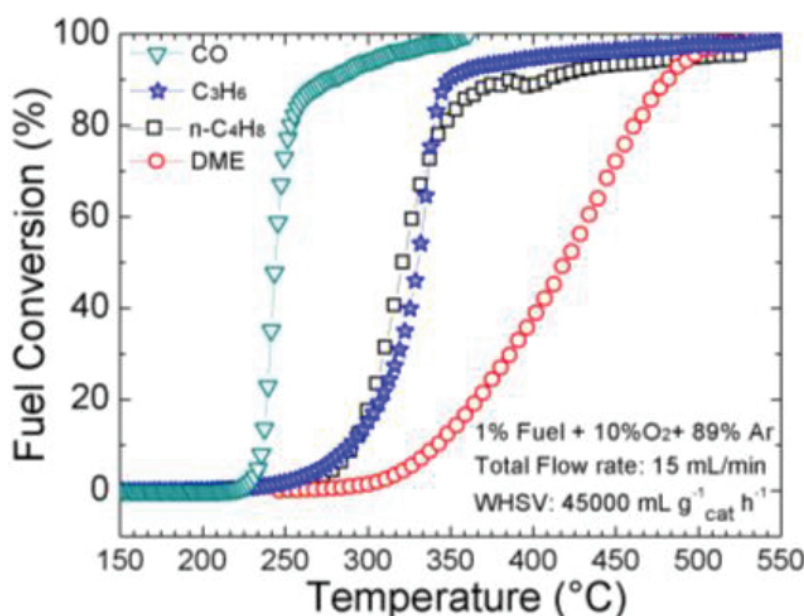

Figure 14. Light-off curves of CO, C_3H_6, n-C_4H_8 and DME oxidation over the PSE-CVD made $CoFe_2O_4$ sample. Reproduced with permission from [26]. Copyright 2015, Wiley-VCH.

For the CO oxidation, the comparison of the temperature at 90% conversion (T_{90}) over $CoFe_2O_4$ (260°C) as catalyst with that obtained with $Co_{0.9}Fe_{2.1}O_4$ (230°C), $Co_{1.8}Fe_{1.2}O_4$ (250°C) and $Co_{2.1}Fe_{0.9}O_4$ (298°C) from our previous work has been made. The results indicate the following performance order: $Co_{0.9}Fe_{2.1}O_4 > Co_{1.8}Fe_{1.2}O_4 > CoFe_2O_4 > Co_{2.1}Fe_{0.9}O_4$. $CoFe_2O_4$ owns similar composition as $Co_{0.9}Fe_{2.1}O_4$, but it exhibits less activity for CO oxidation. By the way, the comparison of the T_{50} of CO over $CoFe_2O_4$ (243°C) with results obtained with Pt/Al_2O_3 (304°C) and $Pt/CoO_x/Al_2O_3$ (340°C) catalysts reported by Torncrona et al. [89] indicates that $CoFe_2O_4$ is more active at low temperature.

In the investigation of the CO oxidation over cobalt ferrite oxides with different composition ($Co_{0.9}Fe_{2.1}O_4$, $Co_{1.8}Fe_{1.2}O_4$ and $Co_{2.1}Fe_{0.9}O_4$) [25], it was established that the performance of cobalt ferrite oxide was not dependent on the variation of the Co content in the mixed oxides. Therefore, these results suggest that CO oxidation over $CoFe_2O_4$ follows a suprafacial mech-

anism where CO molecules react with adsorbed oxygen at the surface of the catalyst to form CO_2. Considering that the difference in the catalytic performance of CO over $CoFe_2O_4$ with seemingly the same composition as $Co_{2.1}Fe_{0.9}O_4$ [25], it was therefore evident that the process is independent on the Co population in the cobalt ferrite oxide, but on the lattice and adsorbed oxygen, mainly adsorbed oxygen at the surface of the material.

The oxidation of C_3H_6 and n-C_4H_8 on $CoFe_2O_4$ starts at temperatures lower than that of DME and the trend for the rate of oxidation is $C_3H_6 \approx n$-$C_4H_8 >$ DME [26]. In the presence of $CoFe_2O_4$ nanoparticles, the oxidation becomes detectable at around 250°C for C_3H_6 and n-C_4H_8 and 285°C for DME and the T_{90} is 334, 371 and 470°C for C_3H_6, n-C_4H_8 and DME, respectively. The temperature at the complete oxidation was 475°C for C_3H_6, 485°C for n-C_4H_8 and 506°C for DME. These values appear to be higher than those for $Co_{2.1}Fe_{0.9}O_4$ catalysts, where complete oxidation was observed at 400, 425 and 446°C for C_3H_6, n-C_4H_6 and DME, respectively [27]. However, they were lower than those observed for C_3H_6 on Au/Al_2O_3 [80] and $La_{1.7}Sr_{0.3}CuO_4S_{0.2}$ [90]. The activity in n-C_4H_8 oxidation was comparable to the measurement on Co_3O_4 [48]. In general, for the oxidation reactions over $CoFe_2O_4$ at low temperatures, no toxic or partial oxidation products are formed when complete conversion of VOCs is achieved. For DME oxidation, it has been established that the reaction network consists of four pathways giving rise to CH_3OH, HCHO, $HCOOCH_3$ and COx [87]. Kouotou et al. [26] detected only CO_2, indicating the higher activity of $CoFe_2O_4$ catalyst for total oxidation of DME at low temperature.

3.2.3. PSE-CVD made $CuCo_2O_4$ for low-temperature catalytic combustion of CO and VOCs

To investigate the potential application of the grown Co-Cu oxides, Tian et al. [28] investigated the catalytic performance of the prepared samples with respect to the total oxidation of CO and C_3H_6. The authors carried out the same tests on bare meshes to exclude the background effect of the mesh structures on the oxidation processes. **Figure 15** compares the light-off curves of CO and C_3H_6 by using Co_3O_4 and Co-Cu oxide referring to the bare mesh. With Co_3O_4, the conversion of CO occurs at 270°C and complete conversion was achieved at 362°C. For Co-Cu oxide, these values shift to 125 and 221°C, respectively. CO oxidation over bare mesh was observed to begin at around 395°C and finish at 833°C. Under similar conditions, CO oxidation on other TMOs such as Mn_3O_4 was reported to happen at 190°C and complete at 343°C [43]. Compared to Mn_3O_4, Co-Cu oxide exhibits better performance. This could be explained by the abundance of adsorbed oxygen, Co^{3+} and Cu^{2+} revealed in the XPS analysis. By applying the Arrhenius equation at low conversion profiles (within 5%), the Ea values were calculated to be 68.2, 77.3 and 82.9 kJ mol^{-1} for the CO oxidation with Co_3O_4, Co-Cu oxide and bare mesh, respectively. As shown in **Figure 15b**, both Co-Cu oxide and Co_3O_4 improve the catalytic oxidation of C_3H_6 compared to the bare mesh. In the presence of Co-Cu oxide, the propene conversion becomes detectable at 220°C. This value was 30 and 120°C lower than that with Co_3O_4 and bare mesh, respectively. With Co-Cu oxide and Co_3O_4, complete conversion of C_3H_6 was reached within 412 and 454°C, while this value was observed to be 772°C for the reaction on NCM. It should be mentioned that CO_2 is the unique measurable product and no trace of CO was detected in the oxidation process with the prepared $CuCo_2O_4$ and Co_3O_4, as

depicted in **Figure 16**. This result agrees well that the conclusion drawn in our recent work that the active transition metal oxides prevent the formation of CO in the oxidation of low-rank hydrocarbons. In the reaction on bare mesh, a large amount of CO peaking at 758°C was produced, which comes from partial oxidation.
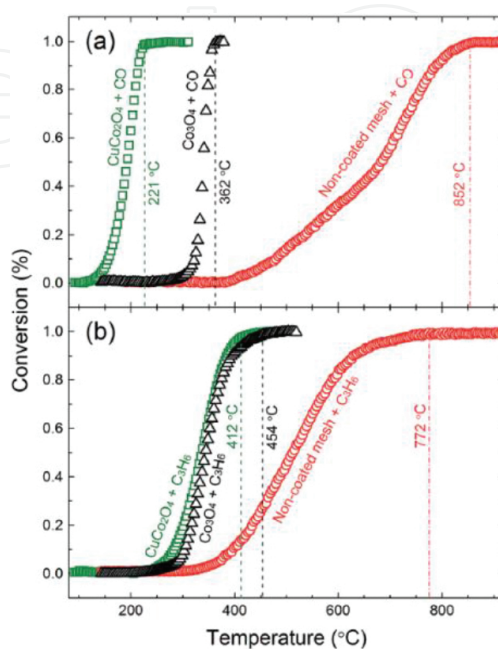

Figure 15. Catalytic performance of Co-Cu oxides: oxidation of CO (a) and propene (b). The reaction was carried at the total flow rate was kept at 15 ml min^{-1} with 1% of fuel and 10% of O$_2$ diluted in Ar, corresponding the WHSV of 75,000 g$_{cat}^{-1}$ h^{-1}. Reproduced with permission from [28]. Copyright 2014, the Royal Society of Chemistry.
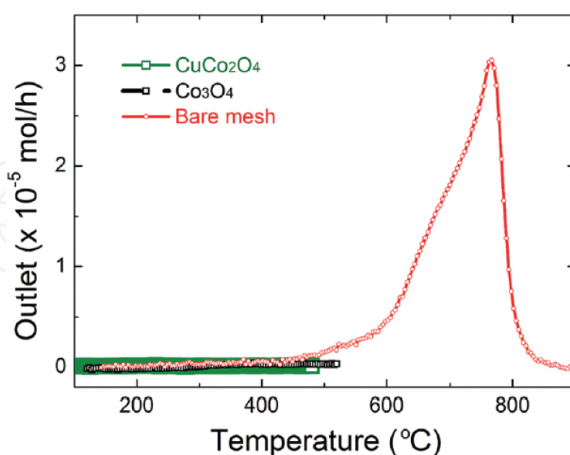

Figure 16. Outlet profiles of CO in the propene oxidation over CuCo$_2$O$_4$, Co$_3$O$_4$ and NCM. Reproduced with permission from [28]. Copyright 2014, the Royal Society of Chemistry.

Compared to the reported T_{50} values in the temperature-programmed reaction, 330°C obtained with CuCo$_2$O$_4$ was lower than that measured with Au/Al$_2$O$_3$ (349°C) [80], Co$_3$O$_4$ (354°C) [48],

Au/MgO/Al$_2$O$_3$ (359°C) [91], La$_{1.7}$Sr$_{0.3}$CuO$_4$S$_{0.2}$ (419°C) [90], (327°C) [91] and Co$_{2.66}$Mn$_{0.34}$O$_4$ (321°C) [24]. Although CuO shows better performance with the T_{50} at 272°C [44], CuCo$_2$O$_4$ has more application prospects than CuO by considering the higher thermal stability. It is worth mentioning that the magnitude order of T_{50} for CuO, CuCo$_2$O$_4$ and Co$_3$O$_4$ follows the order of the band gaps [28]. It can be explained that the migration of O^{2-} from the bulk to the surface gets easier for samples with lower band gaps which have better electron mobility. Moreover, the *Ea* for propene oxidation with CuCo$_2$O$_4$ is 82.6 kJ mol^{-1}, which is lower than that obtained with Co$_3$O$_4$ (130 kJ mol^{-1}) [24], CuO (109.5 kJ mol^{-1}) [44], Co$_{2.66}$Mn$_{0.34}$O$_4$ (115.5 kJ mol^{-1}) [24] as well as the non-catalyzed reaction (138.3 kJ mol^{-1}). The MvK mechanism has been established for CO and propene oxidation over CuO [44], Co–Mn oxides and Co–Fe oxides [25–27]. The same redox behavior could exist in the reaction with Co-Cu oxides.

3.2.4. Comparison of the catalytic performances of binary TMOs with literature

Table 4 compares the catalytic performance of the PSE-CVD made mixed TMOs with that of the selected catalysts in the literature. It can be noted that our catalysts present comparable activity to the other systems. Special attention is paid to the comparison of the catalytic performance with noble metals and transition metal oxides. As can be seen from **Table 4**, noble metals and TMOs (mixed) present attractive results in terms of CO, propene, *n*-butene and DME total oxidation.

Type of catalyst	Material	Weight (mg)	Gas composition	WHSV ^{a} (ml g^{-1} h^{-1})	T$_{10}$ ^{b} (°C)	T$_{50}$ ^{b} (°C)	T$_{90}$ ^{b} (°C)	Refs.
Mixed TMOs	CoFe$_2$O$_4$	20	1% C$_3$H$_6$/10% O$_2$ in Ar	45,000	–	334	–	[26]
	Co$_{2.1}$Fe$_{0.9}$O$_4$				–	348	–	[27]
	CuCo$_2$O$_4$	12	1% C$_3$H$_6$/10% O$_2$ in Ar	75,000	–	330	–	[28]
	Co$_{2.66}$Mn$_{0.34}$O$_4$		2% C$_3$H$_6$/20%O$_2$ in Ar		277	321	356	[24]
	Cu$_{0.72}$Co$_{2.28}$O$_4$	40	13% C$_3$H$_6$/52% O$_2$ in N$_2$	15,000	230	275	>400	[100]
	La$_{1.7}$Sr$_{0.3}$CuO$_4$S$_{0.2}$	200	0.1% C$_3$H$_6$/5% O$_2$ in N$_2$	30,000	368	419	500	[90]
Precious metal	Au/Al$_2$O$_3$	200	1.5% C$_3$H$_6$/4% O$_2$ in He	22,500	288	349	410	[80]
	Au/Al$_2$O$_3$		1% C$_3$H$_6$/9% O$_2$ in He	219,512	–	365	–	[91]
	Au/BaO/Al$_2$O$_3$			250,000	–	290	–	
	Au/Rb$_2$O/Al$_2$O$_3$	200	1% C$_3$H$_6$/9% O$_2$ in He	257,143	–	307	–	
	Au/Li$_2$O/Al$_2$O$_3$			225,000	–	327	–	
	Au/MgO/Al$_2$O$_3$			214,286	–	359	–	
	Ag/Al$_2$O$_3$	50	3% C$_3$H$_6$/10% O$_2$ in N$_2$	12,000	–	–	420	[95]
Mixed TMOs	CeAlO$_3$	100	2% CO/2% O$_2$ in N$_2$	60,000	–	–	465	[97]

Type of catalyst	Material	Weight (mg)	Gas composition	WHSV ^{a} (ml g^{-1} h^{-1})	T_{10} ^{b} (°C)	T_{50} ^{b} (°C)	T_{90} ^{b} (°C)	Refs.
	$CuCo_2O_4$	12	1% CO/10% O_2 89%Ar	75,000	–	190		[28]
	$CoFe_2O_4$	20		45,000	–	–	260	[23]
	$Co_{0.9}Fe_{2.1}O_4$				–	–	230	[25]
	$Co_{2.1}Fe_{0.9}O_4$				–	–	298	
	$Co_{1.8}Fe_{1.2}O_4$				–	–	250	
Precious metals	$Pt/H_2SO_4/ZrO_2$	50	3.5% CO/4%O_2 in N_2	120,000	–	–	290	[98]
	Pt/Al_2O_3	2/200	1% CO/1.38%O_2 in N_2	90,000	–	333	430	[89]
	Au/SiO_2	100	1% CO/99% dry air	12,000	–	337	423	[99]
Mixed TMOs	$CoFe_2O_4$	20	1% n-C_4H_8/10% O_2 in Ar	45,000	–		371	[23]
	$Co_{2.1}Fe_{0.9}O_4$		1% nC_4H_8/10%O_2 in Ar		–	358	402	[27]
Mixed TMOs	$CoFe_2O_4$	20	1% C_2H_6O/10%O_2 in Ar	45,000	–	–	470	[26]
	$Co_{2.1}Fe_{0.9}O_4$		–		356	409		[27]

^{a}: *Weight hourly space velocity*
^{b}: *Temperature at X% conversion (X = 10, 50 and 90 %)*

Table 4. Overview of the catalytic performances of PSE-CVD made binary TMOs compared with the literature.

4. Remarks and perspectives

This review highlights the newly developed CVD approach called PSE-CVD for single and binary TMOs thin films coating and their performances in the catalytic oxidation of CO and VOCs. The advances in the synthesis and properties of single and binary oxides thin films have shown potential applications in several catalytic processes. In this review, we first presented different single oxides fabricated by using a more elaborated CVD method. In particular, the complete oxidation of CO and VOCs over Co_3O_4, CuO/Cu_2O, Fe_2O_3, Cr_2O_3 as well as Mn_3O_4 is comprehensively summarized. In addition, the catalytic activity in CO and VOCs oxidation is systematically compared and it can be well-documented that the CO catalytic oxidation activity is related to either the abundance of active metallic cation sites (Co^{3+}, Cu^{2+}, Fe^{3+}, Cr^{3+} and Mn^{3+}) present in Co_3O_4, CuO/Cu_2O, Fe_2O_3, Cr_2O_3 as well as Mn_3O_4, respectively, or the weakly bonded molecular oxygen species at their surface. On the basis of the present results, we could conclude that the VOCs catalytic oxidation activity of single TMOs is related with either the reactive surface oxygen species or bulk oxygen mobility, reoxidation of metallic cations species and active oxygen vacancies of single oxides.

Regarding binary systems, Co-based binary oxides generally prepared by co-precipitation, impregnation, surfactant-template methods and by combined impregnation and combustion

synthesis were prepared by PSE-CVD and summarized in the present review. The idea was to formulate active and stable mixed oxide based on the performance obtained with single oxide. In fact, Co_3O_4 is known as the most active single oxides for CO and VOCs deep oxidation and the activity strongly depends on Co^{3+}/Co^{2+} redox couple. Compared with pure Co_3O_4 catalysts, the binary oxide catalysts are generally composed of one or more catalytically active components and a functional support, in which the interaction between the catalytic components and the supports can provide improved redox properties and enhanced catalytic behavior [92–94]. As for single oxide catalysts, the active component alone can catalyze the various reactions at a certain kinetic rate, which is usually relatively low. The synergistic effect between binary oxide catalysts leads to the improved catalytic activity. Therefore, the combination of Co and individual metal of single oxide such as Fe_2O_3, Mn_3O_4 and CuO enables the obtaining of binary oxide like Co-Mn-O, Co-Fe-O and Co-Cu-O with new chemical and cationic distribution benefits to the obtained catalytic performances summarized in this review. From the obtained results, it seems like combining two transition metals influence the interaction of active cobalt oxide with the second oxide, affecting the textural and structural properties of the binary oxides. In particular, the investigations of the interaction mechanisms as a function of the surface redox properties of the binary oxides are comprehensively summarized. The catalytic activity of the binary oxides in CO and VOC oxidation is compared and different reaction mechanisms occurring in CO and VOC oxidation are presented. Probably, the surface adsorbed oxygen species over the surface oxygen vacancies of the catalysts are mainly attributed to the CO oxidation activity at low temperatures. The total oxidations of VOCs over transition metal oxides are suggested to follow the MvK redox process.

Nevertheless, in the case of VOCs oxidation, the catalytic activity depends on the nature of catalysts and VOCs. While CO oxidation over single oxide seems to be mainly governed by the amount of available surface oxygen species, VOCs oxidation activity of PSE-CVD made single oxide in contrary is scarcely determined by the surface oxygen species. In the case of CO oxidation, PSE-CVD made single and binary oxides show relevant concentration of surface oxygen species which might be involved in the oxidation at low temperatures. Moreover, the higher activity of Co_3O_4 and $Co_{0.9}Fe_{2.1}O_4$ binary oxides with respect to the Fe_2O_3 or CuO with respect to $CuCO_2O_4$ and other binary oxides is mainly attributed to their higher mobility of lattice oxygen species.

The investigation of the catalytic properties of single and binary TMOs made by PSE-CVD has provide valuable results in the literature, about the employ of a well-established nonconventional CVD approach for the selective synthesis of oxide made of Co, Cu, Fe, Cr and Mn and their performances toward low temptation conversion of CO, C_2H_2, C_3H_6, n-C_4H_8 and C_2H_6O in harmless CO_2 and H_2O. As perspectives, we think that the following aspects deserving further investigations are: (1) further research study of the interactions between different kinds of binary oxide catalytic systems and related corrections between their redox properties and catalytic activities; (2) investigation of the interactions among three or more component catalytic systems, such as noble metal doped or noble metal alloys doped Co-Mn, Co-Fe and Co-Cu binary oxides. It is expected that the novel structures matrix can offer new opportunities to expand our understanding of this kind of interaction as well as relationship between

structure and property; (3) because of his lattice oxygen reservoir character when used as supporter, single Co_3O_4, CuO, Fe_2O_3 crystals structure needs to be deposited on CeO_2 nano-particles in order to control this kind of interaction between these two oxides and to enhance application potentials of these multifunctional materials. It is expected that such an integration of the current investigations on different systems will bring a more comprehensive under-standing of the interactions during the catalytic process and therefore will be of great significance in searching for and find novel multi-oxide catalysts of further enhanced catalytic activity, selectivity as well as durability.

5. Summary

The catalysis science of non-precious metals has significantly improved recently, due to development of more elaborated synthesis approaches for their controlled synthesis and advanced characterization techniques that allow more fundamental insights into the reaction mechanisms. As summary of the present review on the low-temperature oxidation of CO and VOCs over selected non-precious metal such as TMOs catalytic materials either in their single and binary or mixed phases prepared using PSE-CVD, the following main results can be summarized:

1. The catalytic combustion has become the most popular method for the environmental emission control. Thus, catalytic oxidation of CO and VOCs is highly desirable to proceed at low temperature for the consideration of energy savings, low cost, operation safety and environmental friendliness.

2. To reduce the temperature of VOCs catalytic oxidation, great efforts have been made to develop efficient and low cost catalysts via an elaborated synthesis method, namely pulsed spray evaporation chemical vapor deposition. The grid mesh of stainless steel as inert substrates was used instead of catalytically active support to enable the real evalu-ation of the catalytic performance of the as-deposited thin films layer toward CO and VOCs oxidation, offering the major advantage of low-pressure drop.

3. TMOs exhibited comparative activity versus noble metals toward the catalytic oxidation of VOCs at low temperature. The catalytic performance of TMOs was found to be generally affected by many factors such as the composition, the valence of metallic particles, doping, the film morphology and the particle size of the metals oxide.

4. Single oxides systems composed of transition metals (Co, Cu, Cr, Fe and Mn) are efficient for the abatement of CO and VOCs. In addition, the effect of doping should be taken into consideration since they greatly improve the thermal properties and the catalytic per-formances of the as-prepared materials. For instance, the combination of two transition metals or the doping that is the introduction of another transition metal ion in the matrix of single oxides to form a mixed oxide catalysts such as Co-Mn, Co-Fe and Co-Cu oxides also contributes to stabilize the as-deposited catalysts, enable the total oxidation of VOCs and exhaust stream at low temperature.

5. The favored mechanism for CO total oxidation over TMOs catalysts is the suprafacial mechanism, involving reaction between adsorbed molecules on metal sites, while the occurrence of intrafacial mechanism, also known as Mark-van Krevelen mechanism, has been demonstrated for the total oxidation of the representative VOCs (C_2H_2, C_3H_6, n-C_4H_8, C_2H_6O) over TMOs catalysts at low temperature. Therefore, it can be concluded that the validity of each mechanism strongly depends on the redox properties of the catalysts as well as the adsorbed species at the catalyst surface.

6. The comparison of the catalytic performance of PSE-CVD made TMOs with other catalysts reported in the literature indicated that TMOs present comparative activity with some noble metals and mixed oxides like perovskites. Such performances confirm that TMOs should be really considered as potential candidates for the replacement of limited available and high-cost precious metal catalysts.

7. This review validates PSE-CVD as low cost and promising synthesis approach for the control synthesis of active single or mixed TMOs for low-temperature catalytic oxidation of CO and VOCs.

Conflict of interest

The authors confirm that this review article has no conflict of interest.

Acknowledgements

Author details

Patrick Mountapmbeme Kouotou[1,3*], Guan-Fu Pan[1,2] and Zhen-Yu Tian[1,2*]

*Address all correspondence to: patrick@iet.cn and tianzhenyu@iet.cn

1 Intistitute of Engineering Thermophysics, Chinese Academy of Sciences, Beijing, China

2 University of Chinese Academy of Sciences, Beijing, China

3 Higher Institute of the Sahel, University of Maroua, Maroua, Cameroon

References

[1]   R. M. Heck, R. J. Farrauto and S. T. Gulati, Catalytic air pollution control: commercial technology, John Wiley & Sons, 2009.

[2]   S. Scire and L. F. Liotta, *Appl. Catal. B: Environ.*, 2012, 125, 222–246.

[3]   H. Huang, Y. Xu, Q. Fenga and D. Y. C. Leung, *Catal. Sci. Technol.*, 2015, 5, 2649–2669.

[4]   C. He, J. Li, J. Cheng, L. Li, P. Li, Z. Hao and Z. P. Xu, *Ind. Eng. Chem. Res.*, 2009, 48, 6930–6936.

[5]   J. C.-S. Wu and T.-Y. Chang, *Catal. Today*, 1998, 44, 111–118.

[6]   J. Carpentier, S. Siffert, J.-F. Lamonier, H. Laversin and A. Aboukais, *J. Porous Mater.*, 2007, 14, 103–110.

[7]   M. Guillemot, J. Mijoin, S. Mignard and P.Magnoux, *Appl. Catal. B: Environ.*, 2007, 75, 249–255.

[8]   J.-F.Lamonier, A.-B. Boutoundou, C. Gennequin, M. Pérez-Zurita, S. Siffert and A. Aboukais, *Catal. Lett.*, 2007, 118, 165–172.

[9]   J.-M. Giraudon, A. Elhachimi and G. Leclercq, Appl. Catal. B: Environ., 2008, 84, 251–261.

[10] L. F. Liotta, M. Ousmane, G. D. Carlo, G. Pantaleo, G. Deganello, G. Marci, L. Retailleau and A. Giroir-Fendler, *Appl. Catal. A: Gen.*, 2008, 347, 81–88.

[11] S. C. Kim and W. G. Shim, *Appl. Catal. B: Environ.*, 2009, 92, 429–436.

[12] P. O. Thevenin, A. G. Ersson, H. M. J. Kusar, P. G. Menon and S. G. Järas, *Appl. Catal. A: Gen.*, 2001, 212, 189–197.

[13] M. F. M. Zwinkels, S. G. Järas, P. G. Menon and T. A. Griffin, *Catal. Rev. Sci. Eng.*, 1993, 35, 319–358.

[14] M. Baldi, E. Finocchio, F. Milella and G. Busca, *Appl. Catal. B: Environ.*, 1989, 16, 43–51.

[15] M. Labari, S. Siffert, J.-F. Lamonier, E. A. Zhilinskaya and A. Aboukaıs, *Appl. Catal. B: Environ.*, 2003, 43, 261–271.

[16] R. Spinicci, M. Faticanti, P. Marini, S. D. Rossi and P. Porta, *J. Mol. Catal. A: Chem.*, 2003, 197, 147–155.

[17] M. Alifanti, M. Florea, S. Somacescu and V. I. Parvulescu, *Appl. Catal. B: Environ.*, 2005, 60, 33–39.

[18] T. Ataloglou, J. Vakros, K. Bourikas, C. Fountzoula, C. Kordulis and A. Lycourghiotis, *Appl. Catal. B: Environ.*, 2005, 57, 299–312.

[19] B. P. Barbero, J. A. Gamboa and L. E. Cadus, *Appl. Catal. B: Environ.*, 2006, 65, 21–30.

[20] G. K. Boreskov, In: J.R. Anderson, M. Boudart (Eds.), *Catalysis, Science and Technology, vol. 3*, Springer Verlag, New York, 1982.

[21] M. Shelef, K. Otto and H. Gandhi, *J. Catal.*, 1968, 12, 361–375.

[22] Y.-F. Y. Yao, *J. Catal.*, 1974, 33, 108–122.

[23] P. M. Kouotou, Z. Y. Tian, U. Mundloch, N. Bahlawane and K. Kohse-Höinghaus, *RSC Adv.*, 2012, 23, 10809–10812.

[24] Z. Y. Tian, P. H. T. Ngamou, V. Vannier, K. Kohse-Höinghaus and N. Bahlawane, *Appl. Catal. B: Environ.*, 2012, 117–118, 125–134.

[25] P. M. Kouotou, H. Vieker, Z. Y. Tian, P. H. T. Ngamou, A. E. Kasmi, A. Beyer, A. Gölzhäuser and K. Kohse-Höinghaus, *Catal. Sci. Technol.*, 2014, 4, 3359–3367.

[26] P. M. Kouotou and Z. Y. Tian, *Phys. Status Solidi A*, 2015, 212, 1508–1513.

[27] Z. Y. Tian, P. M. Kouotou, A. E. Kasmi, P. H. T. Ngamou, K. Kohse-Höinghaus, H. Vieker, A. Beyer and A. Gölzhäuser, *Proc. Combust. Inst.*, 2015, 35, 2207–2214.

[28] Z. Y. Tian, H. Vieker, P. M. Kouotou and A. Beyer, *Faraday Discuss.*, 2015, 177, 249–262.

[29] M. Kang, M. W. Song and C. H. Lee, *Appl. Catal. A: Gen.*, 2003, 251, 143–156.

[30] M. M. Natile and A. Glisenti, *Chem. Mater.*, 2005, 17, 3403–3414.

[31] L. Xue, C.-B. Zhang, H. He and Y. Teraoka, *Appl. Catal. B: Environ.*, 2007, 75, 167–174.

[32] J. Y. Luo, M. Meng, X. Li, X. G. Li, Y. Q. Zha, T. D. Hu, Y. N. Xie and J. Zhang, *J. Catal.*, 2008, 254, 310–324.

[33] G. Spinolo, S. Ardizzone and S. Trasatti, *J. Electroanal. Chem.*, 1997, 423, 49–57.

[34] J. R. A. Sietsma, J. D. Meeldijk, J. P. d. Breejen, M. Versluijs-Helder, A. J. V. Dillen, P. E. D. Jongh and K. P. D. Jong, *Angew. Chem. Int. Ed.*, 2007, 119, 4631–4633.

[35] Y. F. Yuan, X. H. Xia, J. B. Wu, X. H. Huang, Y. B. Pei, J. L. Yang and S. Y. Guo, *Electrochem. Commun.*, 2011, 13, 1123–1126.

[36] P. H. T. Ngamou and N. Bahlawane, *J. Solid State Chem.*, 2009, 182, 849–854.

[37] J. J. Spivey, *Ind. Eng. Chem. Res.*, 1987, 26, 2165–2180.

[38] M. Boudart and G. Djega-Maxiadassou, Kinetics of Heterogeneous Catalytic Reactions, Princeton University Press: Princeton, N.J.,1984.

[39] C. N. Hinshelwwod, Kinetics of Chemical Change in Gaseous Systems, Clarendon Press, Oxford, 3rd ed., 1933.

[40] P. Mars and D. W. V. Krevelen, *Spec. Suppl. Chem. Eng. Sci.*, 1954, 3, 41–59.

[41] B. Varghese, T. C. Hoong, Z. Yanwu, M. V. Reddy, B. V. R. Chowdari, A. T. S. Wee, T. B. C. Vincent, C. T. Lim and C. H. Sow, *Adv. Funct. Mater.*, 2007, 17, 1932–1939.

[42] C. M. Pradier, F. Rodriguez, P. Marcus, M. V. Landau, M. L. Kaliya, A. Gutman and M. Herskowitz, *Appl. Catal. B: Environ.*, 2000, 27, 73–85.

[43] Z. Y. Tian, P. M. Kouotou, N. Bahlawane and P. H. T. Ngamou, *J. Phys. Chem. C*, 2013, 117, 6218–6224.

[44] Z. Y. Tian, H. J. Herrenbrück, P. M. Kouotou, H. Vieker, A. Beyer, A. Gölzhäuser and K. Kohse-Höinghaus, *Surf. Coat. Technol.*, 2013, 230, 33–38.

[45] G.-F. Pan, S.-B. Fan, J. Liang, Y.-X. Liu and Z. Y. Tian, *RSC Adv.*, 2015, 5, 42477–42481.

[46] J. Liang, G.-F. Pan, S.-B. Fan, W.-L. Cheng and Z. Y. Tian, *Phys. Status Solidi C*, 2015, 12, 1001–1005.

[47] L. F. Liotta, H. Wu, G. Pantaleo and A. M. Venezia, *Catal. Sci. Technol.*, 2013, 3, 3085–3102.

[48] Z. Y. Tian, N. Bahlawane, F. Qi and K. Kohse-Höinghaus, *Catal. Commun.*, 2008, 11, 118–122.

[49] M. Haneda, Y. Kintaichi, N. Bion and H. Hamada, *Appl. Catal. B: Environ.*, 2003, 46, 473–482.

[50] X. C. Jiang and A. B. Yu, *J. Mater. Process. Technol.*, 2009, 209, 4558–4562.

[51] L. P. Zhu, N. C. Bing, L. L. Wang, H. Y. Jin, G. H. Liao and L. J. Wang, *Dalton Trans.*, 2012, 41, 2959–2965.

[52] F. Jiao, A. Harrison, J. C. Jumas, A. V. Chadwick, W. Kockelmann and P. G. Bruce, *J. Am. Chem. Soc.*, 2006, 128, 5468–5474.

[53] J. S. Walker, G. I. Straguzzi, W. H. Manogue and G. C. A. Schuit, *J. Catal.*, 1988, 110, 298–309.

[54] P. M. Kouotou, Z. Y. Tian, H. Vieker, A. Beyer, A. Gölzhäuser and K. Kohse-Höinghaus, *J. Mater. Chem. A*, 2013, 1, 10495–10504.

[55] P. M. Kouotou, Z. Y. Tian, H. Vieker and K. Kohse-Höinghaus, *Surf. Coat. Technol.*, 2013, 230, 59–65.

[56] W. Bergermayer and H. Schweiger, *Phys. Rev. B*, 2004, 69, 195409.

[57] A. Kandalam, P. Jena, S. Khanna, B. Chatterjee and B. V. Reddy, *Am. Phys. Soc. Meeting, March 13–17 (abstract W11.003)*. 2007

[58] S. Wagloehner, D. Reichert, D. Leon-Sorzano, P. Balle, B. Geiger and S. Kurerti, *J. Catal.*, 2008, 260, 305–314.

[59] N. N. Bulgakov and V. A. Sadykov, *React. Kinet. Catal. Lett.*, 1996, 58, 397–402.

[60] X. W. Xie and W. J. Shen, *Nanoscale*, 2009, 1, 50–56.

[61] X. Wang, W. Tian, T. Y. Zhai, C. Y. Zhi, Y. Bando and D. Golberg, *J. Mater. Chem.*, 2012, 22, 23310–23326.

[62] R. J. H. Voorhoeve, J. P. Remeika and D. W. Johnson, *Science* 1973, 180, 62–64.

[63] C. Hu, Q. Zhu, Z. Jiang, L. Chen and R. Wu, *Chem. Eng. J.*, 2009, 152, 583–590.

[64] P. Li, C. Y. Nan, Z. Wei, J. Lu, Q. Peng and Y. D. Li, *Chem. Mater.*, 2010, 22, 4232–4236.

[65] Y. Li, H. Tan, X.-Y. Yang, B. Goris, J. Verbeeck, S. Bals, P. Colson, R. Cloots, G. V. Tendeloo and B.-L. Su, *Small*, 2011, 7, 475–483.

[66] H. Lv, M. G. Yao, Q. J. Li, Z. P. Li, B. Liu, R. Lui, S. C. Lu, D. M. Li, J. Mao, X. L. Ji, J. Liu, Z. Q. Chen, B. Zou, T. Cui and B. B. Liu, *J. Phys. Chem. C*, 2012, 116, 2165–2171.

[67] Y. Chang and J. G. McCarty, *Catal. Today*, 1996, 30, 163–170.

[68] S. C. Kim and W. G. Shim, *Appl. Catal. B: Environ.*, 2010, 98, 180–185.

[69] V. P. santos, M. F. R. Pereire, J. J. M. Orfao and J. L. Figueiredo, *Top. Catal.*, 2009, 52, 470–481.

[70] V. Iablokov, K. Frey, O. Geszti and N. Kruse, *Catal. Lett.*, 2010, 134, 210–216.

[71] E. Finocchio, R. J. Willey, G. Busca and V. Lorenzelli, *J. Chem. Soc. Faraday Trans.*, 1997, 93, 175–180.

[72] P.-O. Larsson, H. Berggren, A. Andersson and O. Augustsson, *Catal. Today*, 1997, 35, 137–144.

[73] G.-H. Lee, M. S. Lee, G.-D. Lee, Y.-H. Kim and S.-S. Hong, *J. Ind. Eng. Chem.*, 2002, 6, 572–577.

[74] Q. Hua, T. Cao, X.-K. Gu, J. Lu, Z. Jiang, X. Pan, L.-F. Luo, W.-X. Li and W. Huang, *Angew. Chem. Int. Ed.*, 2014, 53, 4856–4861.

[75] F. D. Lai, C. Y. Huang, C. M. Chang, L. A. Wang and W. C. Cheng, *Microelectron. Eng.*, 2003, 67–68, 17–23.

[76] E. Sourty, J. L. Sullivan and M. D. Bijker, *Tribol. Int.*, 2003, 36, 389–396.

[77] F. Luo, X. Pang, K. Gao, H. Yang and Y. Wang, *Surf. Coat. Technol.*, 2007, 202, 58–62.

[78] A. G. Tarasov, V. A. Gorshkov and V. I. Yukhvid, *Inorg. Mater.*, 2007, 43, 724–728.

[79] A. Cellard, V. Garnier, G. Fantozzi, G. Baret and P. Fort, *Ceram. Int.*, 2009, 35, 913–916.

[80] S. Ivanova, C. Petit and V. Pitchon, *Gold Bull.*, 2006, 39, 3–8.

[81] Q. Liang, K. D. Chen, W. H. Hou and Q. J. Yan, *Appl. Catal. A: Gen.*, 1998, 166, 191–199.

[82] Q. H. Zhang, X. H. Liu, W. Q. Fan and Y. Wang, *Appl. Catal. B: Environ.*, 2011, 102, 207–214.

[83] D. A. Aguilera, A. Perez, R. Molina and S. Moreno, *Appl. Catal. B: Environ.*, 2011, 104, 144–150.

[84] H. Noller and H. Vinek, *J. Mol. Catal.*, 1989, 51, 285–294.

[85] P. Thormählen, M. Skoglundh, E. Fridell and B. Andersson, *J. Catal.*, 1999, 188, 300–310.

[86] S. Veleva and F. Trifirò, *React. Kinet. Catal. L.*, 1976, 4, 19–24.

[87] H. Liu, P. Cheung and E. Iglesia, *J. Phys. Chem. B*, 2003, 107, 4118–4127.

[88] H. Lee, J. C. Jung, H. Kim, Y. M. Chung, T. J. Kim, S. J. Lee, S. H. Oh, Y. S. Kim and I. K. Song, *Catal. Lett.*, 2009, 131, 344–349.

[89] A. Törncrona, M. Skoglundh, P. Thormählen, E. Fridell and E. Jobson, *Appl. Catal. B: Environ.*, 1997, 14, 131.

[90] M. Machida, K. Ochiai, K. Ito and K. Ikeue, *J. Catal.*, 2006, 238, 58–66.

[91] A. C. Gluhoi, N. Bogdanchikova and B. E. Nieuwenhuys, *J. Catal.*, 2005, 232, 96–101.

[92] S. Hocevar, J. Batista and J. Levec, *J. Catal.*, 1999, 184, 39–48.

[93] C. Kleinlogel and L. J. Gauckler, *Adv. Mater.*, 2001, 13, 1081–1085.

[94] W. J. Shen, Y. Ichihashi and Y. Matsumura, *Catal. Lett.*, 2002, 83, 33–35.

[95] R. Zhang, H. Alamdari and S. Kaliaguine, *Catal. Lett.*, 2007, 119, 108–119.

[96] P. Li, D. E. Miser, S. Rabiei, R. T. Yadav and M. R. Hajaligol, *Appl. Catal. B: Environ.*, 2003, 43, 151–162.

[97] P. A. Deshpande, S. T. Aruna and G. Madras, *Catal. Sci. Technol.*, 2011, 1, 1683–1691.

[98] H. C. Wu, L. C. Liu and S. M. Yang, *Appl. Catal. A: Gen.*, 2001, 211, 159–165.

[99] K. Qian, W. X. Huang, Z. Q. Jiang and H. X. Sun, *J. Catal.*, 2007, 248, 137–141.

[100] H. Baussart, R. Delobel, M. L. Bras and J. M. Leroy, *J. Chem. Soc., Faraday Trans. I*, 1979, 75, 1337–1345.